Peer Review File

Manuscript Title: Three-Dimensional Electronic Microfliers Inspired by Wind-Dispersed Seeds

Editorial Notes:

Reviewer Comments & Author Rebuttals

Reviewer Reports on the Initial Version:

Referee #1 (Remarks to the Author):

A. Key results: Please summarise what you consider to be the outstanding features of the work.
This paper describes the design, fabrication, characterization, and eventual electrical integration of 3D passive fliers at multiple scales (microflier CL<1mm, mesoflier CL~1mm, and macroflier CL>1mm). The authors were inspired by a number of biological examples to motivate their designs and highlight the importance of these small-scale fliers as components in a distributed sensor network, wireless communication nodes, energy harvesting components and/ or various IoT technologies. Their claim is that this paper "introduces the foundational engineering science for practical realization of these ideas."

From the start, I was excited about the possibilities presented in this work. Research labs at Berkeley and Michigan have been developing custom ICs to use in dynamic sensor networks with the hopes that they are light enough to float on air. This work presents flier designs at three different scales that do slow down terminal velocity to allow for larger flight ranges and have rotational behaviors that increase stability of the system. The fabrication methodology allows for the rapid assembly of different flier designs, which in theory could provide different flight trajectories to more efficiently cover an area upon release.

The authors spend the majority of the paper describing the device's flight capabilities (mainly terminal velocity, drag coefficient, and rotational kinematics) through analytical, computational, and experimental processes. I am not an expert in this area, so cannot know for sure, but the authors should spend time explaining whether this is a novel contribution or the application of well-understood analysis to a new flight system.

B. Validity: Does the manuscript have flaws which should prohibit its publication? If so, please provide details.
There are no major flaws that would prevent publication.

C. Originality and significance: If the conclusions are not original, please provide relevant references. On a more subjective note, do you feel that the results presented are of immediate interest to many people in your own discipline, and/or to people from several disciplines?
Overall, I think that this work is significant. Creating small-scale passive fliers is of great interest in the robotics community and this is an interesting platform to achieve these goals. I have two major critiques: first, this paper is very dense, and because there is so much work being presented, the overall message and significant contribution is lost in the detail. A lot of the technical information discussed in the middle of this paper could be moved to the supplemental. Throughout the paper I found myself asking, what lesson did you learn here, or why is this significant, or how does this inform the design specifically? Describing all of the engineering science and analysis isn't convincing, what is the specific insight that the authors developed?

Second, the authors highlight the potential use of many of these devices in a distributed system, but there is little discussion about how this would work. Because the authors spent a lot of time

discussing flow fields, how would these fields affect the flight of an adjacent flier? Could they all be released at the same time? What is the approximate range of these devices (and what applications could you target)? Could you add some asymmetries to achieve directionality? How much sensing/ computation could you reasonably achieve with the current fabrication methods? What size scales are you limited to? What payloads are you limited to? If people wanted to include other sensors or ICs, how could this accomplished? The authors do not need to respond to every idea posed here, but some discussion of the high-level topics would increase interest in other fields.

D. Data & methodology: Please comment on the validity of the approach, quality of the data and quality of presentation. Please note that we expect our reviewers to review all data, including any extended data and supplementary information. Is the reporting of data and methodology sufficiently detailed and transparent to enable reproducing the results?
The approach is quite detailed and covers analytical, computational, and experimental analysis. The fabrication process is detailed and well-cited. In the supplement, it would be nice to include more detailed figure captions. It was difficult flipping between the main text and the supplement to see where the figures were referenced to get a more detailed description of figure content.

Please make sure that all scale bars are correct and that length scales are more readily reported when you call out specific devices. The paper defines ranges, but they are broad. I could not determine the wingspan of the IoT macroflier, and I believe the scale bar in that figure is incorrect (it should be mm not cm).

E. Appropriate use of statistics and treatment of uncertainties: All error bars should be defined in the corresponding figure legends; please comment if that's not the case. Please include in your report a specific comment on the appropriateness of any statistical tests, and the accuracy of the description of any error bars and probability values.
Please define the error bars in all of your figures/ figure captions.
Please report the number of trials in the main text or in the figure where you state probabilities (I believe they are in the supplemental but they should be reported in the main text).

F. Conclusions: Do you find that the conclusions and data interpretation are robust, valid and reliable?
Fine.

G. Suggested improvements: Please list additional experiments or data that could help strengthening the work in a revision.
Please state the wingspan of the devices you highlight. The ranges are helpful but need more specificity when you report specific results.
Also include the mass of the fliers and the payload at each size scale. Could researchers easily incorporate custom ICs or off the shelf devices at different scales?
What are the limitations on adding active electronics to the micro fliers? How much could you add to the mesofliers? What are the power limitations?
At what scale would your analysis no longer hold? How much could another researcher scale up the vehicle to incorporate more active components? How would this affect multi device fabrication and dispersal?
Need more discussion on terms like G_0 and G_1. How do these terms affect the design? What lessons are learned here?
Mentioned above, but what is novel in the analysis of these fliers? Is there a new contribution here or just an application of well-understood ideas?
The three paragraphs from 247 could be moved to the supplemental. It is a lot of technical information about the aerodynamics of the flyer that are not useful to a broad audience.

H. References: Does this manuscript reference previous literature appropriately? If not, what references should be included or excluded?
Fine.

I. Clarity and context: Is the abstract clear, accessible? Are abstract, introduction and conclusions appropriate?
The authors need to provide clearer messaging outside of introducing foundational engineering science. What is the novel contribution? How can this be applied? As I stated above, these fliers are very interesting and the analysis is useful but often feels better suited for a supplemental discussion. What do the authors see as the contribution in the field?

Referee #2 (Remarks to the Author):

The authors describe the creation of 3D fliers over a range of small scales that are inspired by wind dispersed seeds. These fliers are fabricated in a scalable way that can easily create a large number of identical objects. The paper clearly shows that 3D fliers have significantly lower terminal velocities than their 2D precursors through analytical models, CFD, and PIV. The 3D designs employ passive rotation with rudimentary propellers to create lift and slow the fliers descent. The authors also demonstrate that these fliers can be equipped with microelectronic IoT payloads making them useful for environmental monitoring in a variety of scenarios.

The design of these fliers and the accompanying fabrication are an engineering feat that does indeed create a potentially powerful tool in remote sensing. The analysis of the fluid flow induced by these objects is comprehensive and also impressive. The authors clearly show that the 3D fliers rotation creates a stable and low terminal velocity flight that is better at staying aloft than the 2D precursors.

Despite the truly novel and impressive engineering reported in this paper, the connection to the biological inspirations seems somewhat tenuous. The authors show a variety, though not comprehensive set, of wind dispersed fruits in Figure 1a yet each of their designs amounts to essentially a helicopter mechanism of varying size and wing geometry. A comparison across all the classes of fliers they create R, M, H, and PM would also be helpful. Is one design better at some range of Reynolds number or are they all equally effective? The effect of porosity is demonstrated clearly but other comparisons of design class are lacking besides the stark difference between 2D precursors and 3D fliers. No mention is made in the paper comparing their design to the parachute of a dandelion pappus or a fluttering samara and I cannot find any data for their Ribbon fliers in the text. It seems from their analysis that samaras and pappi designs are less effective at reducing falling rate than the helicopter design, yet they are employed frequently in nature nonetheless.

I would recommend that the authors connect their work to comparative work on wind dispersed seeds such as Augspurger AJB vol. 73, p353 (1986). In that paper different drag/lift mechanisms are compared for a wide range of taxa. Moreover Augspurger shows data for a number of seeds that fall at rates only slightly higher than the fliers shown in this paper, which would make a more sensible comparison than the non-wind-dispersed seeds (and snow) shown in Fig. 1(g). Additionally, the authors mention (without citation) in line 123 that wind dispersed seeds maximize stability and dispersal distance, yet their designs outperform these natural counterparts. I don't understand how this can be true if nature is truly maximizing the forces.

I have also noticed a few small errors in the manuscript, which I list below.

In Figure 2, the captions for 2c and 2d are mismatched.

On line 218, the variable Lambda_0 is not defined though it is defined in the SM. The paper would be more readable if it was also defined in the main text.

In Figure S1 and Fig. 1a an array of flier designs is depicted. Is this truly a single photograph as the citations say? It seems like it would be difficult to achieve such clear focus over such a large

depth of field. If these are composite photos the text should indicate that.

In Figure S8a the image is of a dandelion fruit or dandelion pappi, not simply seeds. The species for the feather depicted should also be listed if known.

Equation S1.10 appears to have the lift and drag coefficients upside down in the middle fraction and should read C_L/C_D.

Equation S1.13 also contains an error and, if we use the corrected L_D from above, the last term in parentheses should be (1+L_D^2)^{3/2}, not simply L_D. This equation is repeated in this incorrect form throughout the SM but does not seem to materially affect their analysis since empirical values for C_D are used rather than a value for L_D and Eq. S1.13

Author Rebuttals to Initial Comments:

Referee #1 (Remarks to the Author):

Summary Recommendation: *This paper describes the design, fabrication, characterization, and eventual electrical integration of 3D passive fliers at multiple scales (microflier CL<1mm, mesoflier CL~1mm, and macroflier CL>1mm). The authors were inspired by a number of biological examples to motivate their designs and highlight the importance of these small-scale fliers as components in a distributed sensor network, wireless communication nodes, energy harvesting components and/ or various IoT technologies. Their claim is that this paper "introduces the foundational engineering science for practical realization of these ideas."*

From the start, I was excited about the possibilities presented in this work. Research labs at Berkeley and Michigan have been developing custom ICs to use in dynamic sensor networks with the hopes that they are light enough to float on air. This work presents flier designs at three different scales that do slow down terminal velocity to allow for larger flight ranges and have rotational behaviors that increase stability of the system. The fabrication methodology allows for the rapid assembly of different flier designs, which in theory could provide different flight trajectories to more efficiently cover an area upon release.

Our response: We thank the referee for these positive comments.

Comment #1: *The authors spend the majority of the paper describing the device's flight capabilities (mainly terminal velocity, drag coefficient, and rotational kinematics) through analytical, computational, and experimental processes. I am not an expert in this area, so cannot know for sure, but the authors should spend time explaining whether this is a novel contribution or the application of well-understood analysis to a new flight system.*

Our response: We thank the reviewer for this comment. We agree that the manuscript could benefit from an improved explanation of our analysis approach. The novelty lies in our method of reducing complex 3D shapes into a simplified, discrete number of tilted blades to capture the key physics in compact, analytical forms that reveal scaling behaviors through mathematical connections between the terminal velocities and stability characteristics of fliers and the key geometric and environmental parameters (i.e., G_0, G_1, μ, ρ, etc). As outlined in the manuscript, the results of experimental and computational studies validate these simplified models.

These findings, which include not only the kinematics of the fliers but also the patterns of surrounding air flows, highlight the essential physics that underpins various advantageous aerodynamic properties of 3D fliers over corresponding 2D constructs, including detailed functional dependencies on the 3D architecture. Specifically, the results demonstrate that the symmetricity of the velocity fluctuations and the reduced terminal velocities follow from large induced wakes. Such wakes

generated by naturally occurring wind-dispersed seeds are of great interdisciplinary interest. For example, Cummins et al. *Nature*, **562**, 414–418(2018)) examines wakes induced by dandelion seeds, a parachute type design. Our work focuses on related physics in the context of microsystems inspired by tristellateia seeds, a helicopter type design. This contribution is also novel, in the sense that the flow characteristics of such types of structures (man-made or naturally occurring) have not been examined before.

Our modification to the manuscript: On page 3, line 105, we added "An approach that represents these complex 3D structures as discrete numbers of blades captures the essential physics in simple, analytical scaling forms, validated by computational and experimental results described subsequently."

On page 4, line 115, we changed "Although certain interactions between airborne seeds and the ambient air are well known, few research studies quantitatively define the essential aerodynamics and none considers the potential relevance in microsystems technologies[4-6]" to "Although certain interactions between dandelion seeds and the ambient air are known[13], the flow physics of mediated flight of other classes of wind dispersed seeds, such as tristellateia seeds, are not well understood, nor have they been explored for dispersal of microsystems technologies[14,15]"

13. Cummins, C. *et al.* A separated vortex ring underlies the flight of the dandelion. *Nature* **562**, 414–418 (2018).
14. Rabault, J., Fauli, R. A. & Carlson, A. Curving to Fly: Synthetic Adaptation Unveils Optimal Flight Performance of Whirling Fruits. *Phys. Rev. Lett.* **122**, 24501 (2019).
15. Fauli, R. A., Rabault, J. & Carlson, A. Effect of wing fold angles on the terminal descent velocity of double-winged autorotating seeds, fruits, and other diaspores. *Phys. Rev. E* **100**, 1–13 (2019).

Comment #2: *Overall, I think that this work is significant. Creating small-scale passive fliers is of great interest in the robotics community and this is an interesting platform to achieve these goals. I have two major critiques: first, this paper is very dense, and because there is so much work being presented, the overall message and significant contribution is lost in the detail. A lot of the technical information discussed in the middle of this paper could be moved to the supplemental.*

Our response: We thank the reviewer for this comment. As suggested, we moved much of the technical information in the middle of our manuscript to the supplemental.

Our modification to the manuscript:
The following lists the changes explicitly:

On page 4, line 129, we changed "These designs serve as inspiration for man-made passive flier structures built using approaches introduced here and engineered to optimize aerial dispersal of functional payloads, including a range of electronic, optoelectronic, microfluidic and microelectromechanical systems technologies." to

"These designs serve as inspiration for man-made passive flier structures engineered to optimize aerial dispersal of functional payloads."

On page 5, line 157, we changed "…assembly process on a common substrate. Mass quantities of fliers can be formed at high throughput, as illustrated in Fig. 1f.

The terminal velocity (v_T) associated with free-fall in still air serves as a simple metric to compare the aerodynamics of these fliers to seeds and other objects in nature. As described in the following, microfliers can exhibit values of v_T that are 10 to 15 times small than other objects with similar sizes (~1 mm) and weights (~ 10 mg), including brown rice, sesame seeds, and snow (Fig. 1g)[12]. 3D microfliers with features (diameter ~ 1 mm, mass 12.2 mg, type [3, M, 0.4]) inspired by those of

tristellateia seeds (diameter ~ 19.8 mm, mass 18.2 mg, density ~ 0.11 mg/mm^3; Fig. S2) exhibit v_T ~28 cm/s, which is a factor." to

"…assembly process. Mass quantities of fliers can be formed at high throughput (Fig. 1f). 3D microfliers with terminal velocities (v_T) that are much smaller than other objects with similar sizes and types are possible (Fig. 1g, Supplementary Video 1)[22]."

On page 6, line 167, we changed "Computational Fluid Dynamics (CFD) simulations (see Methods and Extended Data Fig. 2) and analytical approaches (Supplementary Notes 1-4) reveal the underlying aerodynamic mechanisms. The essence of the physics can be examined by decomposing complex flier configurations into discrete numbers of tilted blades, as in Fig. 2a." to

"Computational Fluid Dynamics (CFD) simulations (Methods, Fig. S3) and analytical approaches (Fig. 2a, Supplementary Note 1) capture the underlying aerodynamic mechanisms.

On page 6, line 173, we changed, "Fig. 2b summarizes values of C_{D} computed by CFD at different Reynolds numbers (Re), where $\mathrm{Re} = 2r\rho v_T/\mu$, μ is the dynamic viscosity of air and $2r$ is the diameter of the flier. The results can be described empirically as $C_{\mathrm{D}} \approx G_0 + G_1/\mathrm{Re}$, where the first ($G_0$) and second ($G_1/\mathrm{Re}$) terms correspond to behaviors where inertial and viscous effects dominate, at high and low Re, respectively. The terminal velocity v_T can be then expressed as

$$v_T = -\frac{\mu G_1}{4r\rho G_0} + \sqrt{\left(\frac{\mu G_1}{4r\rho G_0}\right)^2 + \frac{2W}{\rho A G_0}} \qquad (1)$$

where G_0 and G_1 depend on critical geometric parameters of the fliers, …" to

"Fig. 2b summarizes values of C_{D} computed by CFD at different Reynolds numbers ($\mathrm{Re} = 2r\rho v_T/\mu$, where μ is the dynamic viscosity of the air and $2r$ is the diameter of the flier). The empirical relationship $C_{\mathrm{D}} \approx G_0 + G_1/\mathrm{Re}$ applies below the transition region (Re~10^5)[23]. The first (G_0) and second (G_1/Re) terms correspond to the inertial and viscous effects, at high and low Re, respectively. v_T can be expressed as

$$v_T = -\frac{\mu G_1}{4r\rho G_0} + \sqrt{\left(\frac{\mu G_1}{4r\rho G_0}\right)^2 + \frac{2W}{\rho A G_0}} \qquad (1)$$

where G_0 and G_1 depend on geometric parameters of the fliers (Extended Data Fig. 3), …"

On page 6, line 184, we changed, "while for meso- and microfliers, v_T" to

"while for meso- and microfliers,"

On page 7, line 186, we changed, "…consistent with CFD simulations (Fig. S4). As might be expected, the behaviors of microfliers and macrofliers depend mainly on G_0 and G_1, respectively; both parameters are important for mesofliers. The v_T of microfliers and macrofliers depend mainly on μ and ρ, respectively (Fig. S5). The results of CFD (Fig. 2c) show that the flow fields associated with microfliers ($2r$~0.4mm, Re~3; near the Stokes regime) and mesofliers ($2r$~2mm, Re~40) are laminar, while those of macrofliers ($2r$~40mm, Re~3000) are turbulent." to

"…consistent with CFD simulations (Figs. S3-S4). CFD results (Fig. 2c) show that flow fields of microfliers ($2r$~0.4mm, Re~3; near the Stokes regime) and mesofliers ($2r$~2mm, Re~40) are laminar; those of macrofliers are turbulent ($2r$~40mm, Re~3000)."

On page 7, line 192, we changed, "Mesofliers with different 3D configurations exhibit a common dependence of v_T on fill factor (Fig. 2d, Fig. S6, and Supplementary Note 1), $v_T = \frac{4}{\mu G_1}\left(\rho_m t_m g r\sqrt{\eta} + \frac{W_{\mathrm{load}}}{\pi r\sqrt{\eta}}\right)$, as obtained from Eq (3), which is dominated by the viscous term, where W_{load} is the weight of the payload, ρ_m is the density of the structural material, t_m is the thickness, and g is the gravity acceleration. This equation indicates the existence of an optimal fill factor, i.e., $\eta_{\mathrm{optimal}} = W_{load}/\pi r^2 \rho_m t_m g$, that minimizes the terminal velocity for a given W_{load}.

Parachute type seeds incorporate bundles of filaments with high effective porosity $p \approx 0.9$. Such configurations can be mimicked to a certain degree by introducing arrays of perforating holes (i.e., voids) in the structural components of the fliers. The result enhances C_D and reduces v_T [4], with different effects on G_0 and G_1 (Fig. 2b, Figs. S7-S9, and Supplementary Note 2). For example, porosity (e.g.,

$p = 0.25$) has a smaller effect on v_T (by ~ 10%) for macrofliers than for microfliers (by ~ 20%), as shown in Fig. S10." to

"Mesofliers with different 3D configurations have a similar dependence of v_T on η (Fig. 2d, S5), due to thick boundary layers at low Re. Porous features, designed to capture effects of parachute type seeds which incorporate bundles of filaments (e.g., dandelion pappus, $p \approx 0.9$), can be introduced through the addition of perforating holes (i.e., voids) in the structural components of the fliers. The result enhances C_D and reduces v_T , with different effects on G_0 and G_1 (Fig. 2b, Figs. S7-S9, Extended Data Fig. 4 and Supplementary Note 2)[13]. For example, porosity (e.g., $p = 0.25$) has a smaller effect on v_T (by ~ 10%) for macrofliers than for microfliers (by ~ 20%, Fig. S8)."

On page 7, line 206, we changed, "Factors related to the properties of air, i.e., altitude, humidity, temperature or molecular makeup, influence the behaviors mainly through ρ and μ. For example, increasing the altitude from 0 to 80 km decreases ρ by a factor of 5, but the value of μ decreases by less than 25% (Fig. S13). Therefore, as shown by the CFD simulation results in Fig. 2e, mesofliers exhibit small v_T even at high altitudes (e.g., ~ 1.36 m/s at 80 km altitude for $2r \sim 2$ mm). By comparison, macrofliers have large v_T at such altitudes (e.g., > 100 m/s at 80 km altitude for $2r \sim 40$ mm). In a similar way, the temperature and molecular makeup of the air can lead to opposite effects for micro- and macrofliers (Figs. S14 and S15)." to

"Environmental factors, i.e., altitude, humidity, temperature or molecular structure of the air, influence the behaviors mainly through ρ and μ (Figs. S11-S13). For example, increasing the altitude from 0 to 80 km decreases ρ by a factor of 5 and decreases the value of μ by ~25%. Consequently, mesofliers exhibit small v_T even at high altitudes (e.g., ~ 1.36 m/s at 80 km for 2r~2mm, Fig. 2e), far smaller than those of macrofliers at such altitudes (e.g., > 100 m/s for 2r~40mm)."

On page 8, line 214, we changed "Rotational behaviors (e.g., rotational speed ω_T) that follow from the 3D configuration (characterized by β) can confer kinematic stability. Analytical modeling (Supplementary Note 2), validated by CFD (Fig. S16), shows that $\omega_T \propto v_T/r$. With $\beta = 0$, rotation does not occur (Fig. S17). Stability can be analyzed by considering the microflier as a rotating rigid body driven by forces associated with air flow and subjected to small perturbations to its angular speed ($\dot{\Lambda}_1 = \Lambda_0 \cdot 1\text{s}^{-1}$ in direction 1) from an initial balanced state (Fig. 2f and Supplementary Note 4), where Λ_1 and Λ_2 denote the perturbation angles with respect to directions 1 and 2, respectively." to

"Rotational behaviors (e.g., rotational speed ω_T) that follow from the 3D configuration (characterized by β, rotation does not occur with $\beta = 0$) affect v_T by reducing G_1 and increasing G_0 (Extended Data Fig. 5), and by conferring kinematic stability. Analytical modeling (Fig. 2f, Supplementary Note 4) validated by CFD (Fig. S14) shows that $\omega_T \propto v_T/r$."

On page 8, line 220, we changed "Studies of three representative structures (i.e., a 2D precursor; a 3D mesoflier without rotation, i.e., $\beta = 0$, see Fig. S7; and a 3D mesoflier with rotation, all with the same size ($2r \sim 2$ mm) and fill factor ($\eta \approx 0.35$)) reveal the essential effects. " to

"Studies of three representative structures (i.e., a 2D precursor; a 3D mesoflier without rotation; and a 3D mesoflier with rotation, all with the same size ($2r \sim 2$ mm) and fill factor ($\eta \approx 0.35$)) reveal the essential effects. "

On page 8, line 224, we changed "Fig. 2g shows the perturbed angles (Λ_1/Λ_0 and Λ_2/Λ_0) as a function of time (t) after perturbation. The 2D precursor structure does not return to the balanced state. The 3D microflier without rotation returns to the balanced state quickly, but the maximum perturbed angle ($\max\left(\frac{1}{\Lambda_0}\sqrt{\Lambda_1^2 + \Lambda_2^2}\right) \sim 0.025$) is much larger than that of the 3D microflier with rotation ($\max\left(\frac{1}{\Lambda_0}\sqrt{\Lambda_1^2 + \Lambda_2^2}\right) \sim 0.018$). A normalized stability factor, Γ, as defined by

$$\Gamma = \min\left[\text{Real}\left(\left(1 \pm \frac{\omega_0}{\beta_0} i\right) \pm \sqrt{\left(1 \pm \frac{\omega_0}{\beta_0} i\right)^2 - \frac{4\gamma}{\beta_0^2}}\right)\right], \quad (4)$$

can characterize the stability, in which ω_0/β_0 and $4\gamma/\beta_0^2$ account for the influences of material parameters, geometrical parameters and air properties (Fig. 2h, Supplementary Note 4), as given by

$$\beta_0 = \frac{\pi}{8}\frac{\mu r^2}{\sqrt{\eta}} \cdot \mathrm{Re}\left(2G_0 + \frac{G_1}{\mathrm{Re}}\right)\frac{1}{I_1},\ \omega_0 = \frac{I_3 - I_2}{I_1}\omega_T,\ \gamma = \frac{Wd}{I_1}, \quad (5)$$

where $I_{1,2,3}$ are the moment of inertias with respect to directions 1, 2 and 3, and d is the distance between the center of gravity and the center of pressure. A large positive value of Γ suggests that the structure can quickly recover to its balanced, stable state; a negative value of Γ indicates that the structure is unstable. Additionally, the overall maximum perturbed angle, i.e., $\max\left(\frac{1}{\Lambda_0}\sqrt{\Lambda_1^2 + \Lambda_2^2}\right)$, decreases monotonically with ω_0/β_0 (Fig. S18), consistent with rotational improvements in stability. Substitution of Eq. (1) into $\omega_T \propto v_T/r$ suggests that reducing r increases ω_T. As a result, increasing d and/or decreasing r can improve the stability through increases in $4\gamma/\beta_0^2$ and ω_0/β_0." to

"Fig. 2g shows the perturbed angles $(\Lambda_{1,2}/\Lambda_0)$ as a function of time (t) after perturbation. Fig. 2g shows the perturbed angles as a function of time (t) after perturbation. The 2D precursor does not return to the balanced state. The 3D mesoflier without rotation returns to the balanced state quickly, but the maximum perturbed angle (~0.025) is larger than that with rotation (~0.018). A stability factor $\Gamma = \Gamma\left(\frac{\omega_0}{\beta_0}, \frac{4\gamma}{\beta_0^2}\right)$ can be defined to characterize the stability, in which ω_0 $(\propto \omega_T)$, γ and β_0 account for the influence of geometry, material and air properties (Fig. 2h, Supplementary Note 4). A large positive value of Γ corresponds to a structure that can quickly recover to its balanced, stable state; a negative value of Γ corresponds to a structure that is unstable. The maximum perturbed angle decreases monotonically with ω_0/β_0 (Fig. S15), due to rotational improvements in stability."

On page 9, line 239, We changed, "Experimental studies and results of additional computational modeling reveal detailed features of these and related behaviors. One set of measurements involves 3D Particle Tracking Velocimetry (3D-PTV), with a focus on (i) characterizing the 3D trajectories, terminal velocities and the characteristics of aerodynamic stability, and (ii) capturing 3D patterns of flow in a still ambient environment (see Methods, Fig. S19a and Supplementary Video 2 and 3)." To

"Experimental studies reveal detailed features of these and related behaviors. One set of measurements involves 3D Particle Tracking Velocimetry (3D-PTV), with a focus on (i) quantifying the characteristics of aerodynamic stability, and (ii) capturing 3D patterns of flow induced in a quiescent environment (Methods, Extended Data Fig. 6a)."

On page 9, line 252, we changed, "Introducing porosity into the same structure, YP, leads to further reductions in v_T ($v_{T,3D\ porous} \approx 0.28$ m/s; $\eta = 0.26$; Fig. 3b). These results agree with theoretical predictions and simulations, as in Fig. 2c. Across this same set of samples, the 3D shapes reduce the standard deviation of v_T by ~40% due to the enhanced aerodynamic stability ($\sigma_{2D} \approx 0.06$ m/s, $\sigma_{3D} \approx 0.03$ m/s, $\sigma_{3D\ porous} \approx 0.02$ m/s), consistent with the measured trajectories (Fig. 3c). Specifically, the 3D mesofliers travel in a straight downward direction, while the 2D precursors exhibit abnormal, chaotic falling behaviors with a time-dependent combination of fluttering and gliding[13-15]. These latter processes lead to large variations in v_T and in settling location." To

"The addition of porosity into the same structure, YP, promotes further reductions in v_T ($v_{T,3D\ porous} \approx 0.28$ m/s; $\eta = 0.26$; Fig. 3b), consistent with simulations (Fig. 2c). The 3D shapes reduce the standard deviation of v_T by ~40% due to enhanced aerodynamic stability ($\sigma_{2D} \approx 0.06$ m/s, $\sigma_{3D} \approx 0.03$ m/s, $\sigma_{3D\ porous} \approx 0.02$ m/s; Fig. 3c). The 3D mesofliers travel in a straight downward direction, while the 2D precursors exhibit chaotic-like falling[24-26]."

On page 10, line 259, we changed, "The 3D wake structures measured with 3D-PTV highlight additional features. Two representative instants in time (Figs. 3d and Fig. S22) show flow separations, as highlighted by the blue isosurface (flow structures in the opposite direction of the fall) and momentum deficits noted by the red isosurface (flow structures in the direction of the fall). The wake for the 2D flier exhibits comparatively large flow structures against the motion, with small flow structures along the motion at this instant and at other times throughout the fall. The 3D mesoflier induces comparatively small and rotating flow structures oriented against the motion, with large

following structures. Large flow structures against the fall in the 2D precursor indicate early flow separation, which promotes comparatively high pressure gradients and aerodynamic instabilities. Small structures in the direction of the fall indicate small momentum deficits and, consequently, low drag and correspondingly large v_T. The rotational dynamics of the 3D mesofliers minimize flow separation and induce large momentum deficits, resulting in stable and slow falling behaviors (Supplementary Video 6).

Complementary insights follow from high-speed PIV measurements of instantaneous velocity fields (Fig. S23), mean velocity fields (Fig. 3e), velocity profiles (Fig. 3f) and velocity fluctuation profiles (Fig. 3g and h). The 3D mesoflier (Fig. 3e and f, Fig. S23) produces a larger wake and higher vertical velocity fluctuations, σ(u), than the 2D precursor (Fig. 3g). Notably, the fluctuations for the 2D case show asymmetrical distributions due to its planar geometry and nonrotating behavior (Fig. 3h), as additional sources of instability. Symmetry in velocity fluctuations and large momentum deficits are consistent with the enhanced aerodynamics of 3D mesofliers." to

"The 3D wake measured with 3D-PTV further highlights the effects of the rotating 3D mesofliers (Fig. 3d and Supplementary Video 6). Complementary PIV measurements illustrate instantaneous velocity fields (Fig. S19), mean velocity distributions (Fig. 3e), velocity profiles (Fig. 3f) and RMS velocity fluctuation profiles (Fig. 3g-h). The 3D mesoflier (Fig. 3e-f) induces a comparatively larger wake and a higher level of vertical velocity fluctuations, σ(u), compared to the 2D precursor (Fig. 3g). The fluctuations in the 2D case an exhibit asymmetrical distribution due to its nonrotating behavior (Fig. 3h), as a distinct source of instability. Symmetry in velocity fluctuations and large momentum deficits are consistent with the advantageous aerodynamics of the 3D mesofliers."

On page11, line 288, we changed "respectively. The 3D structures are similar to those featured in the CFD simulations (Figs. S24 ~ S28). Layers of polyimide on the bottom and the top enhance the structural integrity of the SMP and improve the rigidity of the overall device. They also place the Si NM near the neutral mechanical plane to minimize the potential for fracture during assembly and use[16,17]." to

"respectively, similar to those featured in the CFD simulations (Figs. S20-S25)."

On page 12 line 322, we changed "Although not explicitly studied in this research, the effects of wind, thermal air currents and fluctuating air flows represent important practical considerations that tend to increase in significance as the sizes and the masses of the fliers decrease. The low terminal velocities of flutterers/spinners are of interest partly because they maximize the time for engagement with these flows, to increase the net transport distance. Gliders and parachuters represent alternative platforms that can be realized using similar constituent materials, fabrication processes, experimental methods and computational techniques. Layouts that combine these various design strategies may offer enhanced levels of performance, beyond those observed in nature. In addition to payloads that support active semiconductor functionality, responsive materials structures that change in color, shape or radio frequency signature according to environmental cues may serve as simple, complementary options for remote monitoring." to

"Although not explicitly studied in this research, the effects of wind represent important practical considerations that tend to increase in significance as the sizes and the masses of the fliers decrease. Gliders and parachuters represent alternative platforms that can be realized using similar approaches. Layouts that combine these various design strategies may offer enhanced levels of performance, beyond those observed in nature."

On page 12, line 310, We changed "Fig. 4f demonstrates the quantitative effect of air-born particles (Fig. S32).

The aerodynamics of these 3D IoT macrofliers (Figs. 4g~i and Fig. S33 ~ S36) are consistent with preceding discussions of the physics. The wakes exhibit oscillating tip vortices in the vicinity of the wings and a secondary vortex behind the center (Fig. 4g and Supplementary Video 7). Mean streamwise velocity fields (Fig. 4h) are similar to those of mesofliers with similar designs. Figure 4i

shows that across a range of centimeter scale dimensions, the normalized transverse velocity profiles exhibit self-similarity, allowing for efficient dimensional analysis and modeling; inferred drag coefficients are shown in Fig. S33c and d)." to

"Fig. 4f demonstrates the quantitative effect of air-borne particles (Extended Data Fig. 9). The aerodynamics of these 3D IoT macrofliers (Figs. 4g-i and Fig. S28-S31) are consistent with preceding discussions of the physics."

On page 15 line 379, we added "Layers of polyimide on the bottom and the top enhance the structural integrity of the SMP and improve the rigidity of the overall device. They also place the Si NM near the neutral mechanical plane to minimize the potential for fracture during assembly and use[16,17]."

On page 16, line 425, we added, "The 3D wake structures measured with 3D-PTV highlight additional features. Two representative instants in time (Figs. 3d and Fig. S17) show flow separations and momentum deficits, as highlighted by the blue (flow structures in the opposite direction of the fall) and red (flow structures in the direction of the fall) isosurfaces, respectively. The wake for the 2D flier exhibits comparatively large and small flow structures against and along the motion, respectively, at this instant and at other times throughout the fall. The 3D mesoflier induces comparatively small and rotating flow structures oriented against the motion, with large following structures. Large flow structures against the fall in the 2D precursor indicate early flow separation, which promotes comparatively high pressure gradients and aerodynamic instabilities. Small structures in the direction of the fall indicate small momentum deficits and, consequently, low drag and correspondingly large v_T. The rotational dynamics of the 3D mesofliers minimize flow separation and induce large momentum deficits, resulting in stable and slow falling behaviors (Supplementary Video 6)."

On page 17, line 452, we added, "The aerodynamics of these 3D IoT macrofliers (Figs. 4g-i and Fig. S27-S30) are consistent with preceding discussions of the physics. The wakes exhibit oscillating tip vortices in the vicinity of the wings and a secondary vortex behind the center (Fig. 4g and Supplementary Video 7). Mean streamwise velocity fields (Fig. 4h) are similar to those of mesofliers with similar designs. Figure 4i shows that across a range of centimeter scale dimensions, the normalized transverse velocity profiles exhibit self-similarity, allowing for efficient dimensional analysis and modeling."

On page 19, line 526, we changed "**g,** The terminal velocity of several small objects and a 3D microflier [3,M,0.4]" to

"**g,** The terminal velocity of several small objects and a 3D microflier [3,M,0.4], inspired by those of tristellateia seeds (diameter ~ 19.8 mm, mass 18.2 mg, density ~ 0.11 mg/mm^3; Fig. S1)."

On page 19, line 530, we added "… decomposing complex flier configurations into discrete tilted blades, …"

On page 20, line 537, we added "Stability can be analyzed by considering the flier as a rotating rigid body driven by forces associated with air flow and subjected to small perturbations ($\dot{\Lambda}_1 = \Lambda_0 \cdot 1\mathrm{s}^{-1}$, where $\Lambda_{1,2}$ denote the perturbation angles in directions 1 and 2, Λ_0 denotes the amplitude) from an initial balanced state ."

On page 20, line 540, we added "$\Gamma \equiv \min\left[\mathrm{Real}\left(\left(1 \pm \frac{\omega_0}{\beta_0} i\right) \pm \sqrt{\left(1 \pm \frac{\omega_0}{\beta_0} i\right)^2 - \frac{4\gamma}{\beta_0^2}}\right)\right]$, where $\beta_0 = \frac{\pi}{8}\frac{\mu r^2}{\sqrt{\eta}} \cdot \mathrm{Re}\left(2G_0 + \frac{G_1}{\mathrm{Re}}\right)\frac{1}{I_1}$, $\omega_0 = \frac{I_3 - I_2}{I_1}\omega_T$, $\gamma = \frac{Wd}{I_1}$. $I_{1,2,3}$ are the moments of inertia for directions 1, 2 and 3, and d is the distance between the center of gravity and the center of pressure."

In Supplementary Note 1, page 3, we added "This equation indicates the existence of an optimal fill factor, i.e., $\eta_{\mathrm{optimal}} = W_{load}/\pi r^2 \rho_m t_m g$, that minimizes the terminal velocity for a given W_{load}."

In Supplementary Note 4, page 8, we added "Substitution of $v_T = -\frac{\mu G_1}{4r\rho G_0} + \sqrt{\left(\frac{\mu G_1}{4r\rho G_0}\right)^2 + \frac{2W}{\rho A G_0}}$ into $\omega_T \propto v_T/r$ suggests that reducing r increases ω_T. Therefore, increasing d (distance between the center of gravity and the center of pressure) and/or decreasing r (size) can improve the stability through increases in $4\gamma/\beta_0^2$ and ω_0/β_0, respectively."

Comment #3: *Throughout the paper I found myself asking, what lesson did you learn here, or why is this significant, or how does this inform the design specifically?*

Our response: We thank the reviewer for this comment. We agree that the lessons learned from these studies should be outlined explicitly. The key findings are that (i) complex bioinspired 3D structures can be designed and manufactured in geometries that create large momentum deficits in wakes induced by free-fall, thereby promoting high drag forces and low terminal velocities, (ii) certain 3D designs induce rotational motions that eliminate instabilities associated with chaotic falling behaviors such as fluttering and tumbling, (iii) the physics associated with (i) and (ii) applies to 3D structures with dimensions in the millimeter range, even for cases near or within the Stokes regime, (iv) analysis approaches that simplify complex 3D configurations into discrete tilted blades can capture the essential physics, including the aerodynamic dependence on the geometric and environmental parameters (i.e., G_0, G_1, μ, ρ, etc.) at different Re.

Our modification to the manuscript:

On page 12, line 321, we added, "The key findings are that (i) complex bioinspired 3D structures can be designed and manufactured in geometries that create large momentum deficits in wakes induced by free-fall, thereby promoting high drag forces and low terminal velocities, (ii) certain 3D designs induce rotational motions that eliminate instabilities associated with chaotic falling behaviors such as fluttering and tumbling, (iii) the physics associated with (i) and (ii) applies to 3D structures with dimensions in the millimeter range, even for cases near or within the Stokes regime, (iv) analysis approaches that simplify complex 3D configurations into discrete tilted blades can capture the essential physics, including the aerodynamic dependence on the geometric and environmental parameters at different Re."

Comment #4: *Describing all of the engineering science and analysis isn't convincing, what is the specific insight that the authors developed?*

Our response: We thank the reviewer for this comment. Our response to Comment #3 addresses this issue.

Our modification to the manuscript:

On page 12, line 321, we added, "The key findings are that (i) complex bioinspired 3D structures can be designed and manufactured in geometries that create large momentum deficits in wakes induced by free-fall, thereby promoting high drag forces and low terminal velocities, (ii) certain 3D designs induce rotational motions that eliminate instabilities associated with chaotic falling behaviors such as fluttering and tumbling, (iii) the physics associated with (i) and (ii) applies to 3D structures with dimensions in the millimeter range, even for cases near or within the Stokes regime, (iv) analysis approaches that simplify complex 3D configurations into discrete tilted blades can capture the essential physics, including the aerodynamic dependence on the geometric and environmental parameters at different Re."

Comment #5: *Second, the authors highlight the potential use of many of these devices in a distributed system, but there is little discussion about how this would work. Because the authors spent a lot of time discussing flow fields.*

Our response: We thank the reviewer for this suggestion, and we agree that some additional explanation would be helpful. The most straightforward schemes for data acquisition from distributed collections of devices involve radio frequency (RF) wireless links to external reader hardware. Options include near field approaches that are common in consumer electronics (Figure 4) and various alternative far field schemes that are used in ultralow-power technologies for IoT applications and wildlife tracking.

As an additional alternative, in further work we demonstrated a remote optical readout concept, in which colorimetric chemical reagents incorporated into the flier structures respond to targeted analytes through changes in color. Aerial digital imaging can then determine the color information for quantitative, wireless data capture – without the need for radio frequency electronics or power supplies. In a simple demonstration, we fabricated collections of 3D microfliers that respond through color change to the pH of the local environment. The indicator consists of an anthocyanin aqueous solution of 0.2 wt% red cabbage extract (Fluxias GmbH), infiltrated into a polycarbonate (PC) membrane (0.2 μm in pore size, 30 μm in thickness, Fisher Scientific). The 3D fliers follow from mechanical transformation of 2D precursors that consist of laser-patterned bilayers of SMP / PC membrane bonded by hot pressing. The envisioned application is in spatial mapping of the pH of surface water associated with lakes, creeks or wetlands through color analysis of aerial photographs.

Our modification to the manuscript: On page 12, line 297, to highlight RF and optical readout approaches for capturing data from a distributed system of fliers, we modified the following sentence "As a simple application example, these types of electronic 3D microfliers can be released into the atmosphere from aircraft to track relevant environmental characteristics from positions at high altitudes to the ground, in large-area, dispersed configurations, as a complement to conventional gravimetric and optical particle counting methods[18,19] performed at stationary, localized positions." to
"These types of electronic and colorimetric 3D meso- and macrofliers can be released into the atmosphere from positions at high altitudes for various applications including atmospheric monitoring, in dispersed configurations, as a complement to conventional gravimetric and optical particle counting methods[18,19] performed at localized positions."

On page 12, line 312, we added "General strategies for data collection from distributed collections of devices involve radio frequency (RF) wireless links to external reader hardware, such as near field (Fig. 4e) and far field schemes that serve as ultralow-power technologies for IoT applications. With colorimetric chemical reagents, readout can occur remotely thorough color analysis of high resolution aerial digital images."

To include our new results on devices and schemes for colorimetric readout, we moved fig. 4b and d to the SI and added the following experimental results into Fig. 4 a,b, and Extended Data Fig. 7..

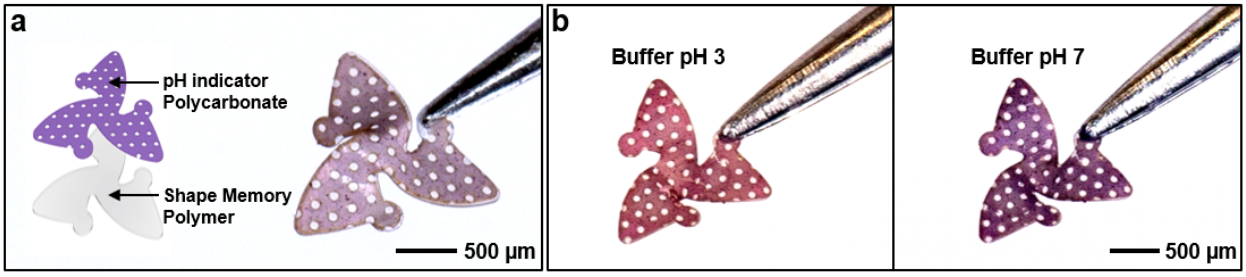

Fig.4| 3D electronic mesofliers, IoT macrofliers and colorimetric mesofliers. **a,** Exploded schematic illustration and images of a colorimetric microflier that responds to local pH. **b**, Color responses of the device at two different pH values.

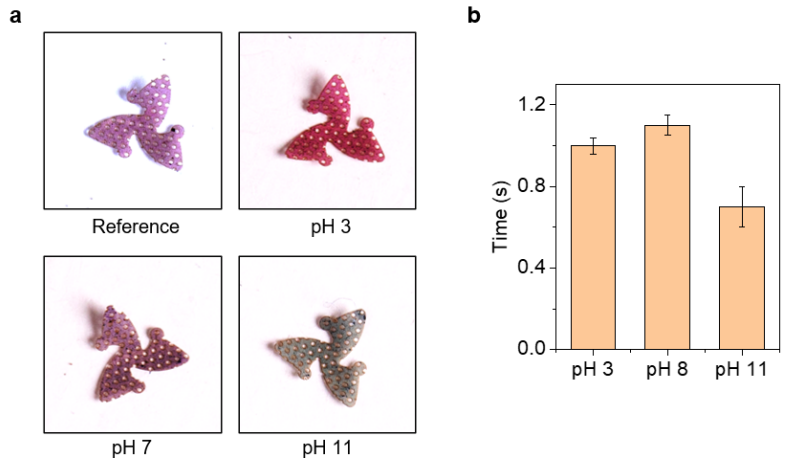

Extended Data Fig. 7. Changes in color of a pH-responsive 3D mesoflier. a, Photographs of pH-responsive 3D mesoflier immersed in different buffer solutions with pH ranging from 3 to 11. **b**, Response time of pH indicators after immersion into buffer solutions at different pH values.

On page 11, line 282, we added a sentence, "As a simple example capable of remote readout without electronics,Fig. 4a and b shows pH-responsive 3D mesofliers [3,M,0.4] that use a color indicator based onanthocyanin infiltrated into a polycarbonate (PC) membrane (Extended Data Fig. 7)[27]".

We added the following to the Method section, "**pH-responsive 3D mesofliers** Fabrication of colorimetric pH-responsive 3D microfliers involved preparation of an anthocyanin aqueous solution of 0.2 wt% red cabbage extract (Fluxias GmbH) and infiltration (~1 mbar) through a polycarbonate (PC) membrane (0.2 μm in pore size, 30 μm in thickness, Fisher Scientific). Mechanical transformation of 2D precursors that consist of laser-patterned (LPKF4 UV laser system) bilayers of SMP / PC membrane bonded by hot pressing yielded the desired 3D structures."

27. Chigurupati, N. *et al.* Evaluation of red cabbage dye as a potential natural color for pharmaceutical use. *Int. J. Pharma.* **241**, 293-299 (2002).

Comment #6: *how would these fields affect the flight of an adjacent flier? Could they all be released at the same time?*

Our response: We thank the reviewer for this interesting comment. In response, we conducted CFD simulations of the interactions between two fliers in parallel free fall, with various lateral separation distances. The results, for structures with dimensions in the range examined in this manuscript, show that the interaction forces become negligible for distance greater than ~10 flier diameters, indicating that the momentum deficit in the wake is fully recovered at the distance of 5 diameters, as confirmed by the experimental results in Fig. 4i. In other words, for separation distances of at least 10 diameters, multiple fliers can be released simultaneously without influence on their individual aerodynamics.

Our modification to the manuscript: On page 12, line 314, we added:
On page 18 line 475, we added "CFD simulations show that multiple fliers can be released simultaneously with non-interacting aerodynamics provided that the separation distances are more than 10 flier diameters, where the wake is fully recovered (Fig. 4i, Fig. S2)."

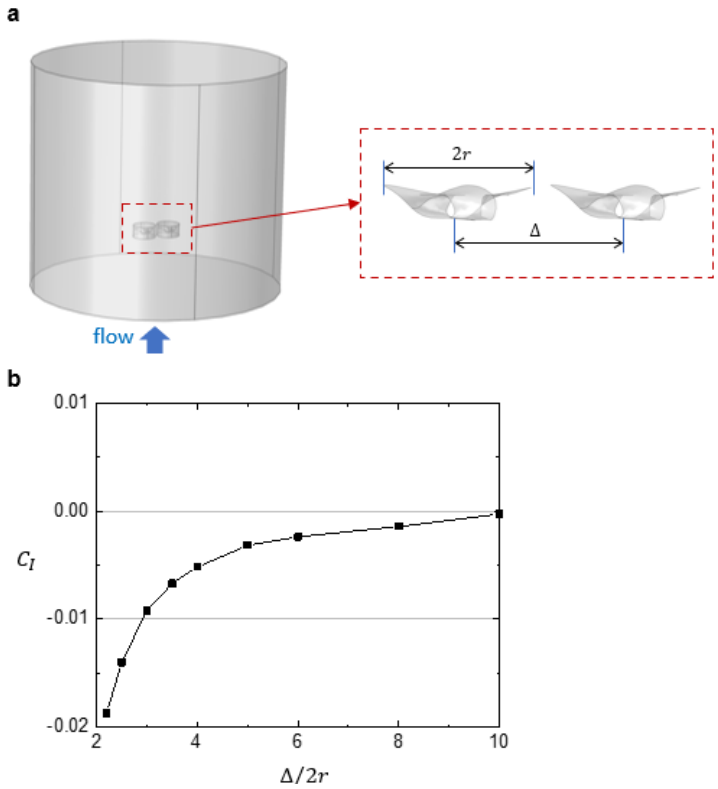

Figure S2. Interaction forces between two mesofliers [3,M,0.4] falling in parallel at their terminal velocities (Re~41). (a) Schematic diagram of the falling mesofliers, with center-to-center distance Δ. (b) Normalized interaction force $C_I = F_I/(0.5\rho v_T^2 A)$ versus the normalized distance $\Delta/2r$, with F_I denotes the interaction force.

Comment #7: *What is the approximate range of these devices (and what applications could you target)?*

Our response: We thank the reviewer for this comment. The 3D fliers can support various types of wireless readout schemes, ranging from near and far field RF approaches to colorimetric imaging methods. The applications span a broad range, depending on the sensor designs, the computational capabilities, the data storage systems, the power supply strategies and others. The approximate ranges for several communication strategies are below. For each case, the detector hardware strongly influences the capabilities, e.g. size of the receiver antenna; the performance of the receiver amplifier, etc. The estimates below are conservative.

(i) Near-Field Communication (NFC) technologies have a range of ~1 m [R1].
(ii) Bluetooth Low Energy (BLE) technologies have a range of ~100 m [R2].
(iii) Radio-Frequency Identification (RFID) technologies have different ranges depending on the designs, from ~2 m to ~5 m, ~100 m, and ~10 km for chipless, passive, active, and very high frequency (VHF) tags respectively [R3].
(iv) Optical technologies, such as those based on colorimetric readout, have a range of tens of km's.

Our modification to the manuscript: On page 11, line 282, we modified "…many possibilities in functional integration, spanning nearly all forms of planar microsystems and semiconductor technolgoies." To "…many possibilities in functional integration, spanning nearly all forms of planar microsystems, semiconductor technologies and wireless components (Table S2)."

We added Table. S2

Table S2. Types of possible electronic components and wireless systems integrated on 3D meso- and macro-fliers.

Types and # of possible electronic components integrated on 3D mesoflier	Silicon CMOS 5×10^9 transistors	Solid-State Memory 10^{11} bits	Solar Cell 4 units	Miniature Lasers 10^6 units	mm-scale Computer 4 units

Types of possible wireless systems integrated on 3D IoT macroflier	Near-Field Communication (NFC)	Bluetooth Low Energy (BLE)	Radio-Frequency Identification (RFID)	Optical Technology (colorimetric readout)
Effective Distance	~ 1 m	~100 m	~2 m (chipless tag) ~5 m (passive tag) ~ 100 m (active tag) ~10 km (very high frequency tag)	A range of tens of km's
The Size of Miniaturized Antenna	5-10 mm	1-2 mm	10~50 mm	N/A

[R1] Jawad, A. M. *et al.* Opportunities and Challenges for Near-Field Wireless Power Transfer: A Review. *Energies*, **10**, 1022, (2017).

[R2] Park, S. I. *et al.* Ultraminiaturized photovoltaic and radio frequency powered optoelectronic systems for wireless optogenetics. *J. Neural Eng.* **12**, 056002, (2015).

[R3] Xuan, X. *et al.* A Miniaturized Meandered Dipole UHF RFID Tag Antenna for Flexible Application, *Int. J. Antennas Propag.* 2951659, (2016).

Comment #8: *Could you add some asymmetries to achieve directionality?*

Our response: We thank the reviewer for this comment. Yes, fliers can be fabricated with asymmetric designs. In additional work, we built "glider" type mesoflier, inspired by *Alsomitra Macrocarpa*, as illustrated below. These structures exhibit directional motion.

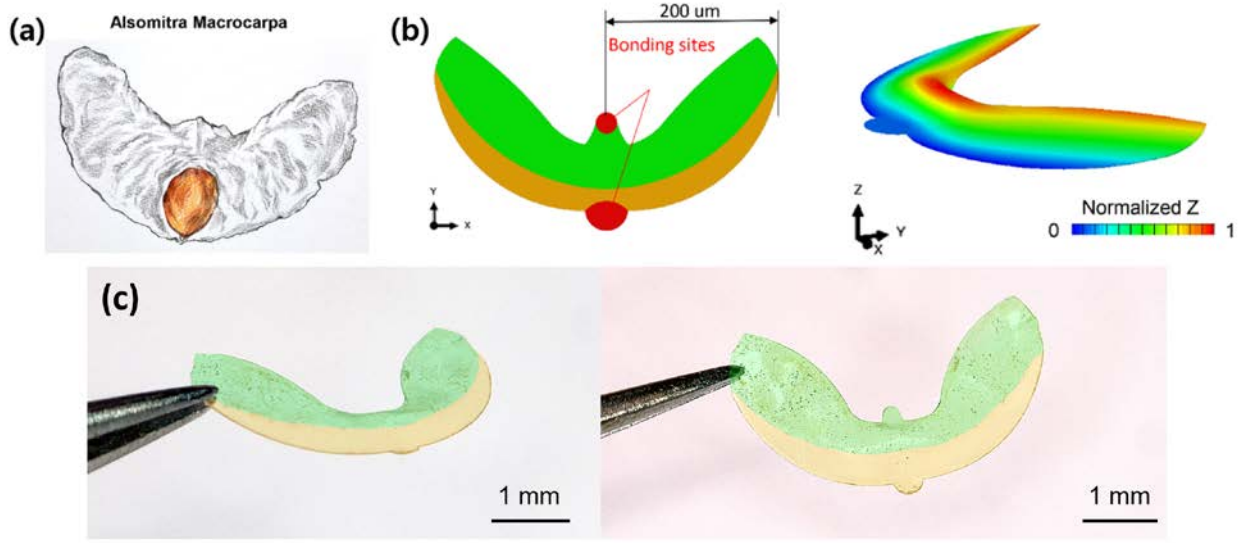

Glider Type 3D Flier. (a), a photograph of *Alsomitra Macrocarpa*. (b), mechanical simulation results of a 3D microflier inspired by *Alsomitra Macrocarpa*. (c) photographs of fabricated 3D mesoflier inspired by *Alsomitra Macrocarpa.*

Comment #9: *How much sensing/computation could you reasonably achieve with the current fabrication methods? What size scales are you limited to? What payloads are you limited to? If people wanted to include other sensors or ICs, how could this accomplished? The authors do not need to respond to every idea posed here, but some discussion of the high-level topics would increase interest in other fields.*

Our response: We thank the reviewer for this comment. We list some examples of sensing/computation capabilities and size/payloads that can be incorporated easily:

i) Silicon CMOS: state of the art in integrated circuit technology allows for 5 x 10^9 transistors per square millimeter on substrates with thicknesses of <1 mm [R4].
ii) Solid-State Memory: state of the art in solid state memory technology allows for 10^{11} bits per square millimeter on substrates with thicknesses of <1 mm [R5].
iii) 'Smart Dust': recent reports describe cubic millimeter scale systems with temperature, light/acceleration sensors, 8-bit ADC and bidirectional optical communication capabilities [R6,R7].
iv) Solar Cells: quadruple-junction, four-terminal solar cells can be produced with thicknesses of tens of microns and lateral dimensions of 600 μm x 600 μm, with solar energy conversion efficiencies of ~45% [R8].
v) Miniature Lasers: optically pumped multi-color lasers based on InGaN/GaN micro disk resonators are available with thicknesses of 500 nm and lateral dimensions of 1 μm x 1 μm [R9]. Another option is vertical cavity surface emitting lasers (VCSELs) similar to those used in smart phones for LiDAR technology. The latest commercial devices have sizes of 250 x 250 μm and thicknesses of 100 μm.
vi) CMOS cameras: camera modules used in smart phones are available with thicknesses of 7.5 μm and 5 μm as well as lateral dimensions of 10 μm x 10 μm and 10 μm x 10 μm for silicon photodiode and micro lens per pixel, respectively.

[R4] Gonzalez-Zalba, M. F. *et al*. Scaling silicon-based quantum computing using CMOS technology: State-of-the-art, Challenges and Perspectives. *Quantum Physics*, November 25, (2020).
[R5] Zahoor, F. *et al*. Resistive Random Access Memory (RRAM): an Overview of Materials, Switching Mechanism, Performance, Multilevel Cell (mlc) Storage, Modeling, and Applications. *Nanoscale Res. Lett.*, **90**, (2020).
[R6] Cook, B. W. *et al*. SoC Issues for RF Smart Dust. *P. IEEE* **94**, 1177, (2006).
[R7] Wu, Xiao, et al. A 0.04 mm 3 16nW wireless and batteryless sensor system with integrated Cortex-M0+ processor and optical communication for cellular temperature measurement. IEEE Symposium on VLSI Circuits, IEEE (2018).
[R8] Sheng, X. *et al*. Printing-based assembly of quadruple-junction four-terminal microscale solar cells and their use in high-efficiency modules. *Nat. Mater*. **13**, 593, (2014).
[R9] Athanasiou, M. *et al*. Monolithically multi-color lasing from an InGaN microdisk on a Si substrate. *Sci. Rep*. **7**, 10086, (2017).

Our modification to the manuscript: Please refer to our modification to the manuscript for ***Comment #7***.

Comment #10: *The approach is quite detailed and covers analytical, computational, and experimental analysis. The fabrication process is detailed and well-cited. In the supplement, it would be nice to include more detailed figure captions. It was difficult flipping between the main text and the supplement to see where the figures were referenced to get a more detailed description of figure content.*

Our response: We thank the reviewer for this comment. We modified the SI captions as follows:

Our modification to the manuscript: On Figure S2, we changed "**A tristellateia seed.** Top-view and cross section view photographs of a tristellateia seed." To "**A tristellateia seed.** Optical images of a tristellateia seed from top and front views. The terminal velocity is ~100 cm/s."

On Figure S5, we changed "**Effect of air properties.** Dependence of terminal velocity on (a) the density and (b) the dynamic viscosity of air for multi-scale fliers." To "**Effect of air properties.** Dependence of terminal velocity on (a) the density and (b) the dynamic viscosity of air for multi-scale fliers. The behavior of the macrofliers depend mainly on the density; the behaviors of the meso- and microfliers depend mainly on the dynamic viscosity."

On Figure S6, we changed "**Amended dependence of the vertical-direction drag force of a 3D mesoflier on the fill factor at small Reynolds number (Re~40).** (a) Schematic diagram of the simplified mesoflier model with various fill factors. (b) Weight to terminal velocity ratio versus fill factor for a mesoflier at small Reynolds number." To "**Amended dependence of the vertical-direction drag force of a 3D mesoflier on the fill factor at small Reynolds number (Re~40).** (a) Schematic diagram of the simplified mesoflier model with various fill factors. (b) Weight to terminal velocity ratio versus fill factor for a mesoflier at small Reynolds number. The results follow from the fitting law $F_z \propto \sqrt{\eta}$."

On Figure S9, we changed "**Velocity fields for airfoil with 3 different porosities (p=0, 0.5 and 0.9).** (a) low Re and (b) high Re. The boundary layers at low Re are shown by velocity contours at $|u|/v_2 = 0.1$." To "**Velocity fields for airfoil with 3 different porosities (p=0, 0.5 and 0.9).** (a) low Re and (b) high Re. The boundary layers at low Re are shown by velocity contours at $|u|/v_2 = 0.1$. At low Re, the boundary layer surrounding the airfoil, which can be seen as a virtual airfoil, is not affected by the porosity on the flat airfoil. The drag force acting on the airfoil is therefore not significantly decreased."

On Figure S10, we changed "**Terminal velocity versus porosity (p) for micro- and macrofliers.** The terminal velocity for the microflier is validated by experimental falling tests (Fig. 3b)." To "**Terminal velocity versus porosity (p) for micro- and macrofliers.** The terminal velocity for the microflier is validated by experimental falling tests (Fig. 3b). Porosity design is more effective on microfliers than on macrofliers."

On Figure S11, we changed "**Effect of airfoil curvature for fliers at high Reynolds numbers.** (a) Scheme of airfoil (cross section of a blade) with different curvatures. (b) ω/v_t and (c) G_0 versus blade tilt angle with different airfoil curvatures (from flat to curved), at large Reynolds numbers." To "**Effect of airfoil curvature for fliers at high Reynolds numbers.** (a) Scheme for airfoils (cross section of a blade) with different curvatures. (b) ω/v_T and (c) G_0 versus blade tilt angle with different airfoil curvatures (from flat to curved), at high Re ~3000. With curvature $c/r_0 = 0.5$, G_0 can be increased by ~35% compared to the flat blade."

On Figure S12, we changed "**Effect of tilt angles of blades on G_0 and G_1.** (a) Scheme of the simplified flier model with different tilt angles (β). The effect of tilt angle on (b) G_0 and (c) G_1." To "**Effect of tilt angles of blades on G_0 and G_1.** (a) Scheme of the simplified flier model with different tilt angles (β). The effect of tilt angle on (b) G_0 and (c) G_1. Optimizing the tilt angle (rotational behavior) will slightly increase G_0, but decrease G_1."

On Figure S14, we changed "**Effect of air properties.** Effect of air temperature on terminal velocity." To "**Effect of air properties.** Effect of air temperature on terminal velocity. The terminal velocity of macro- and microfliers follow from different dependence on the air temperature, because μ increases but ρ decreases with temperature increasing."

On Figure S15, we changed "**Effect of molecular makeup.** Prediction of CFD for small and large fliers falling in different gases. The different μ and ρ indicate the macro- and microfliers follow from different dependence on different molecular makeups." To "**Effect of molecular makeup.** CFD simulations for small and large fliers falling in different gases. The different μ and ρ indicate macro- and microfliers show a different dependence on molecular makeup of the gas. For example, In He, the microflier has the smallest v_T among all gases, but macroflier falls quickly in this same environment."

On Figure S17, we changed "**Mechanical simulation of a 3D microflier [3,H,0.75].** Schematic images of (a) a parachute design where the blades have no rotational tilting, and (b) a rotating flier design with rotationally tilted blades." To "**Mechanical simulation of a 3D microflier [3,H,0.75].** Schematic images of (a) a parachute design where the blades have no rotational tilting, and (b) a rotating flier design with rotationally tilted blades. (c) Comparison of G_0 and G_1 between the parachute mode and rotational falling mode. Rotational behaviors (e.g., rotational speed ω_T) that follow from the 3D configuration (characterized by β, rotation does not occur with $\beta = 0$) can affect v_T by reducing G_1 and increasing G_0."

On Figure S16, we changed "**Scaling law for the terminal rotating speed of a flier.** The rotating speed ω_T versus v_T/r, and the CFD results show a linear relationship, consistent with the analytic model." To "**Scaling law for the terminal rotating speed of a flier.** The rotating speed ω_T versus v_T/r, and the CFD results show a linear relationship, consistent with the analytic model $\frac{\omega_T r}{v_T} = \frac{C_{L(b)}}{C_{D(b)}} = L_D$."

On Figure S18, we changed "**Maximum perturbed angle.** $\max\left(\frac{1}{\Lambda_0}\sqrt{\Lambda_1^2+\Lambda_2^2}\right)$ versus ω_0/β_0 and $4\gamma/\beta_0^2$." To "**Maximum perturbed angle.** The maximum perturbed angle $\max\left(\frac{1}{\Lambda_0}\sqrt{\Lambda_1^2+\Lambda_2^2}\right)$ versus ω_0/β_0 and $4\gamma/\beta_0^2$, where $\beta_0 = \frac{\pi}{8}\frac{\mu r^2}{\sqrt{\eta}} \cdot \mathrm{Re}\left(2G_0 + \frac{G_1}{\mathrm{Re}}\right)\frac{1}{I_1}$, $\omega_0 = \frac{I_3 - I_2}{I_1}\omega_T$, $\gamma = \frac{Wd}{I_1}$. $I_{1,2,3}$ are the moment of inertias for directions 1, 2 and 3, and d is the distance between the center of gravity and the center of pressure. Rotation with higher $\omega_0 \propto \omega_T$ will lead to lower $\max\left(\frac{1}{\Lambda_0}\sqrt{\Lambda_1^2+\Lambda_2^2}\right)$, indicating the rotational stability."

On Figure S21, we changed "**Free-falling a 2D precursor and 3D mesoflier.** (a) Free-falling 2D precursor, (b) Free-falling 3D mesoflier. Instantaneous 3D flow velocity fields induced by free-falling (c) 2D precursor and (b) 3D mesooflier via 3D-PTV. The color denotes the in-plane 2D vertical velocity along the flier's center plane. Red and blue-sio-surfaces demonstrate iso-values of 15 and -5 mm/s, respectively." To "**Free-falling 2D precursor and 3D mesoflier.** (a) Free-falling 2D precursor, (b) Free-falling 3D mesoflier. Instantaneous 3D flow velocity fields induced by free-falling (c) 2D precursor and (b) 3D mesoflier measured via 3D-PTV. The color denotes the in-plane 2D vertical velocity along the flier's center plane. Red and blue-sio-surfaces demonstrate iso-values of 15 and -5

mm/s, respectively. The rotational dynamics of the 3D mesofliers minimize flow separation and induce large momentum deficits, resulting in stable and slow falling behaviors"

On Figure S22, we changed "**CFD simulated vertical flow field.** (a) A 2D precursor and (b) 3D mesoflier [3,M,0.4] (Size scale 2r ~ 2 mm)." To "**CFD simulated vertical flow field.** (a) A 2D precursor and (b) 3D mesoflier [3,M,0.4] (Size scale 2r ~ 2 mm). The simulation agrees well with the experimentally measured flow field."

On Figure S23, we changed "**Experimental results for mesoflier.** Instantaneous velocity fields induced by fixed (a) 2D precursor and (b) 3D mesoflier via PIV above the wind tunnel." To "**Experimental results for mesoflier.** Instantaneous velocity fields induced by a fixed (a) 2D precursor and (b) 3D mesoflier via PIV above the wind tunnel. Flow fields induced by the 3D mesoflier exhibit a larger momentum deficit than the 2D precursor."

On Figure S24, we changed "**Simulations for 3D mesofliers design I [3,M,0.4].** FEA showing (a) 2D precursor and (b) 3D configuration for the mesoflier. (c) Deflection of the 3D mesoflier during free-fall at the terminal velocity. The deflection is magnified by 1000 times. (d) CFD results for the terminal velocity as a function of the mass of the mesoflier." To "**Simulations for 3D mesoflier design I [3,M,0.4].** FEA showing (a) 2D precursor and (b) 3D configuration for the mesoflier. (c) Deflection of the 3D mesoflier during free-fall at the terminal velocity. The deflection is magnified by 1000 times. (d) CFD results for the terminal velocity as a function of the mass of the mesoflier. The deflection of the mesoflier during free fall at the terminal velocity has only a slight effect on its 3D configuration."

On Figure S26, we changed "**A 3D IoT macroflier with another design.** (a) Mechanical simulation results and (b) photographs with a circuit to measure fine dust pollution through the light dosimetry method." to "**A 3D IoT macroflier with another design.** (a) Mechanical simulation results and (b) photographs with a circuit to measure fine dust pollution through the light dosimetry method. The mechanical simulation guides the design and well predicts the fabricated configuration of the IoT macroflier. The weight of this flier is 14.6 mg (d~4cm), with payload 75.4mg."

On Figure S27, we changed "**Effect of thickness on the deflection of 3D IoT macrofliers during falling.** 3D IoT macrofliers with design of (a) Fig. 4e and (b) Fig. S24, respectively." To "**Effect of thickness on the deflection of 3D IoT macrofliers during falling.** 3D IoT macrofliers with (a) IoT design I and (b) IoT design II, respectively. A thick SMP layer >12 μm can limit the deflection of the structure to <2 mm for IoT fliers (2r ~ 20mm) during falling."

On Figure S28, we changed "**Electromagnetic simulations.** Inductance and Q-factor for 3D IoT macrofliers with design of (a) Fig. 4e and (b) Fig. S24 for 2D/3D configuration, respectively." To "**Electromagnetic simulations.** Inductance and Q-factor for 3D IoT macrofliers with (a) IoT design I and (b) IoT design II for 2D/3D configuration, respectively. Electromagnetic simulations guide the designs of the antennas and prove the feasibility."

On Figure S34, we changed "**CFD results for a 3D IoT macroflier.** (a) Instantaneous velocity field. (b) Mean velocity field in the streamwise direction u/U." To "**CFD results for a 3D IoT macroflier.** (a) Instantaneous velocity field. (b) Mean velocity field in the streamwise direction u/U. The CFD simulation agrees well with the PIV results."

On Figure S35, we changed "**PIV results for 3D IoT macrofliers.** Mean velocity field of (a) 1cm, (b) 2cm, (c) 3cm, (d) 4cm, and (e) 5 cm-diameter 3D IoT macrofliers at incoming velocity *U*=1.2m/s. Velocity profiles along the (f) center-axis and (g) spanwise direction at 12 diameter downstream." To "**PIV results for 3D IoT macrofliers.** Mean velocity field of (a) 1cm, (b) 2cm, (c) 3cm, (d) 4cm, and (e) 5 cm-diameter 3D IoT macrofliers at an incoming velocity *U*=1.2m/s. Velocity profiles along the (f) center-axis and (g) spanwise direction at a position corresponding to 12 flier diameters downstream. The results show characteristics of self-similarity."

Comment #11: *Please make sure that all scale bars are correct and that length scales are more readily reported when you call out specific devices. The paper defines ranges, but they are broad. I could not determine the wingspan of the IoT macroflier, and I believe the scale bar in that figure is incorrect (it should be mm not cm).*

Our response: We thank the reviewer for this comment and apologize for the typo. Yes, the scale bar of the 3D IoT macroflier on fig.4e should be 5 mm, not 5 cm. We corrected it.

Comment #12: *All error bars should be defined in the corresponding figure legends; please comment if that's not the case. Please include in your report a specific comment on the appropriateness of any statistical tests, and the accuracy of the description of any error bars and probability values. Please define the error bars in all of your figures/ figure captions.*

Our response: We thank the reviewer for this comment. The only error bars presented in this work are in fig. 3b and the represent the standard deviation for the terminal velocities of the 2D precursor, 3D mesoflier and porous 3D mesoflier. We added a definition of the error bar in fig. 3b.

Our modification to the manuscript: In figure 3b, we changed, **"b**, Mean terminal velocity and its standard deviation for Y2 = a 2D precursor for a 3D mesoflier [3,M,0.4] and 3D mesoflier Y = [3,M,0.4], and YP = a porous 3D mesoflier for [3,PM,0.4]." to
"b, Mean terminal velocity (square symbol; □), and standard deviation (error bar) for Y2 = a 2D precursor for a 3D mesoflier [3,M,0.4] and 3D mesoflier Y = [3,M,0.4], and YP = a porous 3D mesoflier for [3,PM,0.4]".

Comment #13: *Please report the number of trials in the main text or in the figure where you state probabilities (I believe they are in the supplemental but they should be reported in the main text).*
Our response: We thank the reviewer for this comment. We modified the text as follows.

Our modification to the manuscript: In figure 3b, we changed, "… YP = a porous 3D mesoflier for [3,PM,0.4]" to
"… YP = a porous 3D mesoflier for [3,PM,0.4]; total number of trials for each case is, N=10".

Comment #14: *Please state the wingspan of the devices you highlight. The ranges are helpful but need more specificity when you report specific results. Also include the mass of the fliers and the payload at each size scale.*

Our response: We thank the reviewer for this comment. We listed the wingspan and mass of the meso- and microfliers featured in Figure 1-3 in the Table S1. A microscale inorganic LED with a weight ~120 nN serves as the payload for the mesofliers. We added this information in the caption of Fig. 2. The weight the IoT fliers are 19.7 mg for Fig. 4e (d~5cm, payload 198mg), and 14.6 mg for Fig. S23 (d~4cm, payload 75.4mg).

Our modification to the manuscript: On page 19, line 523, we added "The values for the masses of micro- and mesofliers are listed in Table S1. "

We added Table S1:

Table S1. Mass of fliers at meso- and microscales.

Flier Designs	Meso- (d~2 mm)	Micro- (d~0.5 mm)
[2,R,0.2]	4.82 μg	0.301 μg
[2,H,0.6]	9.63 μg	0.602 μg
[2,H,1.2]	20.5 μg	1.28 μg
[3,H,0.6]	13.9 μg	0.872 μg
[3,H,0.75]	9.49 μg	0.593 μg
[3,M,0.4]	12.2 μg	0.763 μg
[3,PM,0.4]	9.16 μg	0.573 μg
[3,M,0.33]	11.5 μg	0.718 μg
[3,R,0.5]	6.73 μg	0.421 μg

On page 20, line 533, we added "…, with microscale inorganic LED (~120 nN) as an optional payload."

On page 21, line 566, we added "The weight of IoT flier is 19.7 mg (d~5cm), with payload 198mg."

In caption of Fig. S23, we added "The weight of this flier is 14.6 mg (d~4cm), with payload 75.4mg (Fig. S23)."

Comment #15: *Could researchers easily incorporate custom ICs or off the shelf devices at different scales?*

Our response: We thank the reviewer for this comment. Yes, custom ICs or off-the-shelf devices can be easily integrated onto fliers with appropriate sizes, as discussed in Comment #7 and #9. One must, however, consider effects of their mass, volume, shape, etc, on the detailed aerodynamics, to enable associated optimizations in design.

Our modification to the manuscript: Please refer to our modification to the manuscript for ***Comment #7***.

Comment #16: *What are the limitations on adding active electronics to the micro fliers?*

Our response: We thank the reviewer for this comment. The main limitations follow from considerations in size and weight. For active electronics with RF communication capabilities, the size of the antenna is often a dominating consideration. For NFC, the antenna dimensions can be as small as 5-10 mm; for BLE, the antenna dimensions can be as small as 0.5-1 mm. Other important components are those associated with power harvesting (e.g. solar cells) and/or storage (e.g. batteries).

Our modification to the manuscript: Please refer to our modification to the manuscript for ***Comment #7***.

Comment #17: *How much could you add to the mesofliers?*

Our response: We thank the reviewer for this comment. We demonstrated the addition of microscale inorganic LED to the mesofliers as representative payloads, with weight of ~120 nN. Larger payloads

can be incorporated but at the expense of increased terminal velocities. See fig. S4 for details. For example, an IC component with a weight of 630 nN added to the mesoflier [3,M,0.4] will increase v_T by ~200%. We added this detail in the Caption of Figure 2d.

Our modification to the manuscript: We changed the caption of Fig. 2c:
"c, Terminal velocities of four different 3D mesofliers X = [3,H,0.75], Y = [3,M,0.4], Z = [3,H,0.6], and W = [2,H,1.2] with various fill factors, with microscale inorganic LED (~120 nN) as an optional payload. "

Comment #18: *What are the power limitations?*

Our response: We thank the reviewer for this comment. We agree with the need to include some comments on power supply. One option is in wireless power transfer. For NFC coupling, we can expect to deliver up to 10 mW into the IoT flier from standard transmission antennas in the high frequency band and RF hardware. Similarly, for far field power transfer in the ultra-high frequency band, practical limits are in the 20-35 mW range using dipole antennas using a similar RF power harvester system from the previous work [R10]. Another option is in batteries. Chip-scale lithium ion batteries (Enerchip CBC005, Cymbet) have dimensions of 1.75 mm x 2.15 mm, weights of 100 mg, with output voltages 3.8 V and capacities of 5μAh. Miniature button cell batteries (GRP3013020-X2A, Grepow) have dimensions of 6 mm x 6 mm, weights of 1.1g, with output voltages of 4.2 V and capacities of 37 mAh. A third possibility is in solar energy harvesting. With the types of microscale, multijunction cells (size of 600 μm x 600 μm) mentioned previously, one can expect to harvest 100 mW [R11] over areas comparable to the IoT flier.

As presented in our 3D IoT flier platform, combining an NFC coil with a passive dosimetry circuit that includes photodiodes and supercapacitors as a battery-free, wireless device. Here, photodiodes (~75 mg) ARE and supercapacitors (~25 mg) arranged in electrical parallel continuously transduce and store electromagnetic radiation (EMR) in the form of electrical energy [R12]. The accumulated potential across the supercapacitor serves as a measure of EMR exposure, as a form of spectroscopic characterization of the atmosphere that does not require a battery for operation. Wireless data transfer involves NFC coupling to an external reader. In additional work, we examined the detailed electromagnetics associated with this process.

[R10] Huang, X. *et al.* Epidermal radio frequency electronics for wireless power transfer. *Microsyst. Nanoeng.* **2.1**, 1-9, (2016).
[R11] Sheng, X. *et al.* Printing-based assembly of quadruple-junction four-terminal microscale solar cells and their use in high-efficiency modules. *Nat. Mater.* **13**, 593, (2014).
[R12] Heo, S. Y. et al. Wireless, battery-free, flexible, miniaturized dosimeters monitor exposure to solar radiation and to light for phototherapy. *Sci. Transl. Med.*, **10** (470), (2018).

Our modification to the manuscript: On page 18, line 477, we changed,
"The commercial software ANSYS HFSS was used to perform electromagnetic finite element analysis and to determine the inductance, Q factor for the 2D and 3D antennas. Lumped ports yielded the port impedance Z of the antennas. An adaptive mesh (tetrahedron elements) and a spherical radiation boundary (radius of 1000 mm) ensured computational accuracy. The inductance (L) and Q factor (Q) (shown in Fig. S28) were obtained from L = Im/(2πf) and Q = |Im/Re|, where Re4, Im4 and f represent the real and imaginary part of the Z and the frequency, respectively. The default material properties included in the HFSS material library were used in the simulation." to
"The commercial software ANSYS HFSS was used to perform electromagnetic finite element analysis and to determine the inductance, Q factor for the 2D and 3D antennas. Lumped ports yielded the port impedance *Z* of the antennas. An adaptive mesh (tetrahedron elements) and a spherical radiation boundary (radius of 1000 mm) ensured computational accuracy. The inductance (L) and Q factor (Q)

(shown in Fig. S28) were obtained from L = Im{Z} /(2πf) and Q = |Im{Z} /Re{Z}|, where Re{Z}, Im{Z}, and f represent the real and imaginary part of the Z and the operating frequency, respectively. The approximate power P_{out} in the flier coil is calculated from the S-parameters (shown in Extended Data Fig. 10) by varying the vertical distance between the coil and a high-frequency (HF) transmission antenna as

$$\eta_{21} = \frac{P_{out}}{P_{in}} = \frac{|S_{21}|^2(1-|\Gamma_L|^2)}{[1-|(1-|\Gamma_L|^2)|^2](|1-S_{22}\Gamma_L|^2)} \cdot 100 \qquad \text{(Eq. XX)}$$

where, P_{in} is the power of the transmission antenna, $\Gamma_L = \frac{Z_L - Z_0}{Z_L + Z_0}$ is the reflection coefficient from the load, Z_L is the impedance of the load, and $Z_0 = 50\ \Omega$ is the reference impedance. The default material properties included in the HFSS material library were used in the simulation.

We added Extended Data Fig. 10.

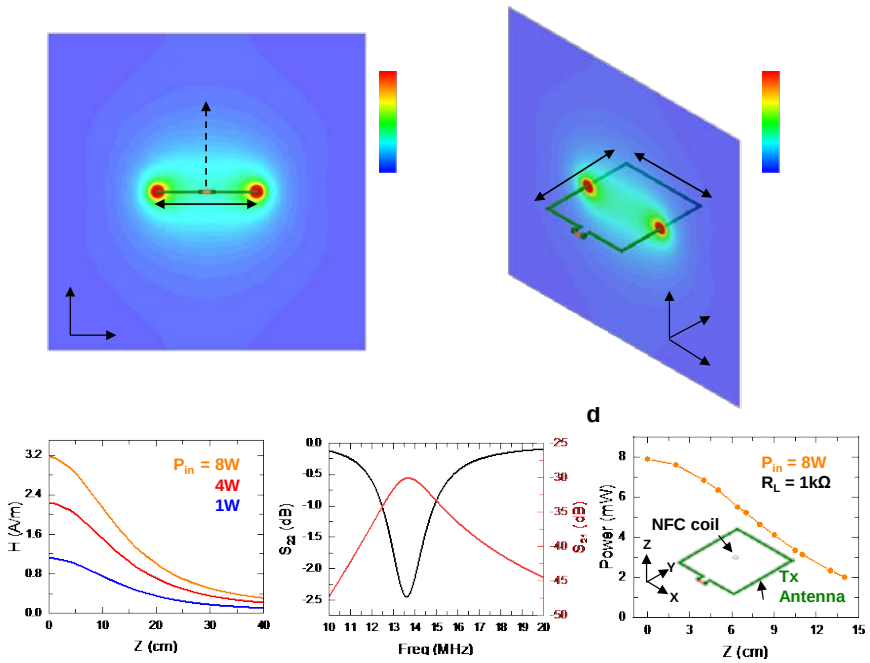

Extended Data Fig. 10. Electromagnetic performance of coils for wireless power transmission. (a) Normalized magnetic field generated by the commercial transmission antenna with dimensions (31.8 cm x 33.8 cm x 3 cm). (b) Magnetic field strength along the line (0,0,Z) as a function of the distance Z normal to the transmission antenna for different input power P_{in} (1, 4, and 8 W). (c) Scattering parameters for the electromagnetic energy transfer between the coils when the NFC coil is located at the center of the transmission antenna (0,0,0). (d) Simulated power in the NFC coil at different distance Z normal to the primary antenna with $P_{in} = 8W$.

Comment #19: At what scale would your analysis no longer hold?

Our response: The theoretical analysis holds when the empirical equation $C_D \approx G_0 + G_1/\mathrm{Re}$ is satisfied, i.e., when Re is below the transition region (Re~10^5, e.g.,) [R13]. Scaling up the devices with Re over the transition region, equation (3) still holds but the value of G_1 should be recalculated with respect to Re. For example, for a 3D macroflier with d~80 cm and v_T~2 m/s, Re~1.1×10^5, the empirical equation $C_D \approx G_0 + G_1/\mathrm{Re}$ no longer holds. 3D microfliers in smaller scales still follow from this equation in Stokes Regime, but molecular movements might play a role at an even smaller scales, i.e. nanofliers

Our modifications to the manuscript: On page 6, line 175, we modified "…can be described empirically as $C_D \approx G_0 + G_1/\mathrm{Re}$, where…" to
"…The empirical relationship $C_\mathrm{D} \approx G_0 + G_1/\mathrm{Re}$ applies below the transition region ($\mathrm{Re} \sim 10^5$)[23]. The…"

23. Hölzer, A. & Sommerfeld, M. New simple correlation formula for the drag coefficient of non-spherical particles. *Powder Technol.* **184**, 361–365 (2008).

Comment #20: How much could another researcher scale up the vehicle to incorporate more active components? How would this affect multi device fabrication and dispersal?

Our response: The basic 3D fabrication approach applies equally well at large scales, up to systems with dimensions in the range of meters, as reported previously in other contexts[18]. Scaling up the device will not affect the multi-device fabrication and dispersion behaviors. For additional detail on dispersal, please refer to our response for ***Comment #6***.

18. Zhang, Y. *et al.* Printing, folding and assembly methods for forming 3D mesostructures in advanced materials. *Nat. Rev. Mater.* **2**, (2017).

Our modifications to the manuscript: On page 14 line 359, we added "The basic 3D fabrication approach applies equally well at large scales, up to systems with dimensions in the range of meters[18]."

Comment #21: Need more discussion on terms like G_0 and G_1. How do these terms affect the design? What lessons are learned here?

Our response: We agree with the referee that G_0 and G_1 are interesting terms guiding the design of fliers and that some additional explanation is needed. According to equation (2), for those of fixed weight, fliers with larger G_1 have smaller terminal velocities at small Reynolds numbers, and similarly for G_0 at large Reynolds numbers. These parameters depend strongly on the design, specifically the 3D configurations of the fliers. In response to the referee's comment, we studied the values of G_0 and G_1 for all classes of flier designs listed in Figure 1c. All structural factors, such as porosity, blade tilt angle and blade curvature, are incorporated in G_0 and G_1 , as demonstrated in Supplementary Notes 1-3. Requirements for higher or lower values of these parameters (G_0 and G_1) can be realized through different design choices. We added Figure Extended Data Fig. 3 and modified the text as follows.

Our modifications to the manuscript: In page 7, line 179, we modified "where G_0 and G_1 depend on critical geometric parameters of the fliers, …" to
"where G_0 and G_1 depend on geometric parameters of the fliers (Extended Data Fig. 3),"

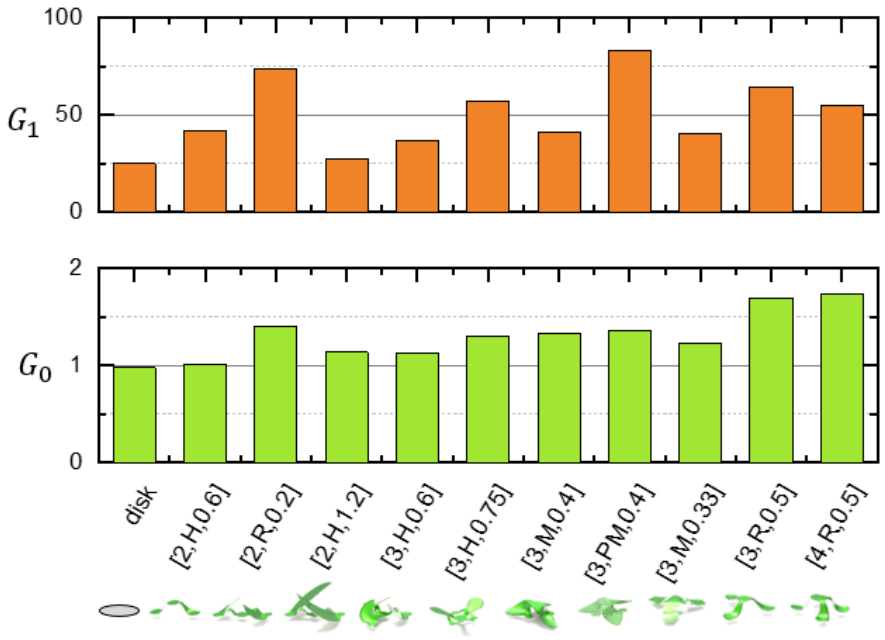

Extended Data Fig. 3. Comparison of G_0 and G_1 across all classes of fliers. CFD Simulation results for the components G_0 and G_1 of the drag coefficient C_D, for fliers of types R, H, M and PM, with the 2D disk as a comparison.

Comment #22: Mentioned above, but what is novel in the analysis of these fliers? Is there a new contribution here or just an application of well-understood ideas?

Our response: We thank the reviewer for this comment. The analytical approach of simplifying complex 3D geometries into discrete numbers of tilted blades represents a novel route to characterize the terminal velocity and stability of fliers and their dependence on key geometric and environmental parameters (i.e., G_0, G_1, μ, ρ, etc.). Please refer to our response for Comment #3 and #4 for more details.

Comment #23: The three paragraphs from 247 could be moved to the supplemental. It is a lot of technical information about the aerodynamics of the flyer that are not useful to a broad audience. The authors need to provide clearer messaging outside of introducing foundational engineering science. What is the novel contribution? How can this be applied? As I stated above, these fliers are very interesting and the analysis is useful but often feels better suited for a supplemental discussion.

Our response: We thank the reviewer for this comment. As suggested, we reduced the fluid modeling/analysis sections by half by moving content to the supplemental information. Please refer to our response for ***Comment #2*** for additional detail**.**

Comment #24: What do the authors see as the contribution in the field?

Our response: We thank the reviewer for this comment. We feel that the main contribution is in defining a bio-inspired concept for distributing microsystems technologies for purposes in monitoring, tracking, surveillance and others. Additionally, we establish new fundamental insights into the essential aerodynamics of free-falling mesoscale objects, and simplified analytical forms that capture the underlying physics. The combined results will appeal to a wide spectrum of researchers, from various

areas of mechanical and aerospace engineering, electrical engineering, materials science and biomedical engineering to plant biology [R14, R15].

[R14] Lentink, D., Dickson, W. B., van Leeuwen, J. L. & Dickinson, M. H. Leading-edge vortices elevate lift of autorotating plant seeds. *Science* **324**, 1438–1440 (2009).
[R15] Greene, D. F. & Johnson, E. A. The aerodynamics of plumed seeds. *Funct. Ecol.* **4**, 117–125 (1990).

Referee #2 (Remarks to the Author):

Summary Recommendation: *The authors describe the creation of 3D fliers over a range of small scales that are inspired by wind dispersed seeds. These fliers are fabricated in a scalable way that can easily create a large number of identical objects. The paper clearly shows that 3D fliers have significantly lower terminal velocities than their 2D precursors through analytical models, CFD, and PIV. The 3D designs employ passive rotation with rudimentary propellers to create lift and slow the fliers descent. The authors also demonstrate that these fliers can be equipped with microelectronic IoT payloads making them useful for environmental monitoring in a variety of scenarios.*
The design of these fliers and the accompanying fabrication are an engineering feat that does indeed create a potentially powerful tool in remote sensing. The analysis of the fluid flow induced by these objects is comprehensive and also impressive. The authors clearly show that the 3D fliers rotation creates a stable and low terminal velocity flight that is better at staying aloft than the 2D precursors.

Our response: We thank the referee for providing these valuable suggestions. We carefully addressed all of the issues, as listed below, and we revised our manuscript accordingly.

Comment #1: *Despite the truly novel and impressive engineering reported in this paper, the connection to the biological inspirations seems somewhat tenuous. The authors show a variety, though not comprehensive set, of wind dispersed fruits in Figure 1a yet each of their designs amounts to essentially a helicopter mechanism of varying size and wing geometry. A comparison across all the classes of fliers they create R, M, H, and PM would also be helpful. Is one design better at some range of Reynolds number or are they all equally effective?*

Our response: We thank the reviewer for this comment. In response, we added CFD simulation results of G_0 and G_1 for all classes of designs (R, M, H and PM) listed in Figure 1c. These key parameters determine the terminal velocities at low and high Reynolds numbers, respectively, as shown in Extended Data Fig. 3. Designs with higher G_0 or G_1 are structurally more effective in reducing the terminal velocity at high or low Reynolds numbers, respectively. All classes of fliers have similar G_0 values of around 1~2. The ribbon designs [3,R,0.5] and [4,R,0.5] have the highest values. Designs [3,PM,0.4], [2,R,0.2] and [3,R,0.5] have the highest G_1. Despite this aerodynamic advantage, we did not use the ribbon fliers as platforms to support electronic components because their small areas limit the payloads. As such, the choice of optimal flier design depends on payload requirements. Analysis in Fig. 2d indicates that the maximum capability of mesofliers to carry payloads involves an optimal fill factor $\eta_{\text{optimal}} = W_{load}/\pi r^2 \rho_m t_m g$. For a flier with payload similar to its own weight (~120 nN), the optimal value is η_{optimal}≈0.35, which is comparable to those of designs [3,M,0.4] and [3,PM,0.4]. Payloads that are smaller than the weight of the flier will reduce the value of the optimal fill factor, to regimes where the ribbon fliers are more effective.

In additional work, we investigated another type of a wind-dispersed seed, not reported in the manuscript -- a "glider" type microflier, inspired by *Alsomitra Macrocarpa*, configured to fly in a directional sense (please see the figure below).

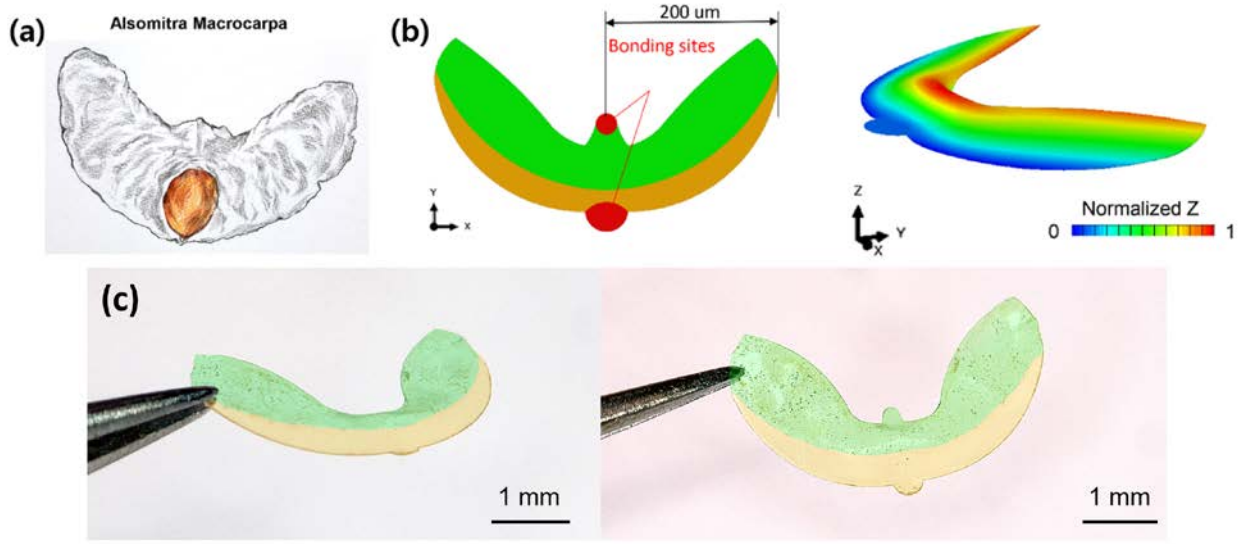

Glider Type 3D Flier. (a), a photograph of *Alsomitra Macrocarpa*. (b), mechanical simulation results of a 3D microflier inspired by *Alsomitra Macrocarpa*. (c) photographs of fabricated 3D mesoflier inspired by *Alsomitra Macrocarpa.*

Our modifications to the manuscript: In page 7, line 179, we modified "where G_0 and G_1 depend on critical geometric parameters of the fliers, …" to
"where G_0 and G_1 depend on geometric parameters of the fliers (Extended Data Fig. 3),"

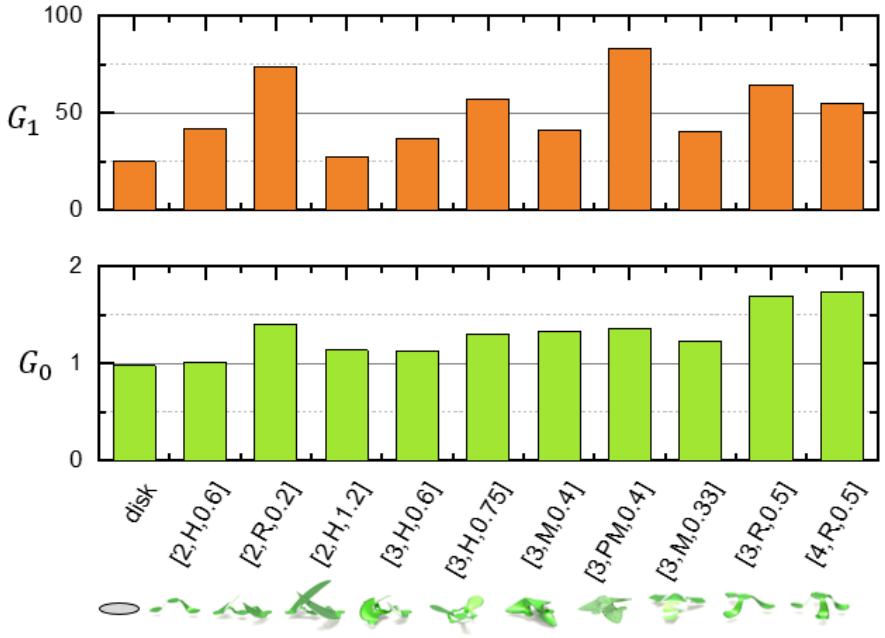

Extended Data Fig. 3. Comparison of G_0 and G_1 across all classes of fliers. CFD Simulation results for the components G_0 and G_1 of the drag coefficient C_D, for fliers of types R, H, M and PM, with the 2D disk as a comparison.

Comment#2: *The effect of porosity is demonstrated clearly but other comparisons of design class are lacking besides the stark difference between 2D precursors and 3D fliers.*

Our response: We thank the reviewer for this comment. For microfliers at small Reynolds numbers, we found that all classes of 3D configurations exhibit a common dependence of terminal velocity on fill factor (Fig. 2d). In other words, the structural effects are almost eliminated by the thick boundary layer due to the viscous effect in the Stokes region. Porosity is effective mainly because it further reduces the weight of the fliers without changing the aerodynamic property at small Re. As a result, porosity represents a different aspect of structural design compared to ribbon and membrane designs.
At large Reynolds numbers, the structural effects are much more complicated. In this work, we discussed the structural effects in terms of their essential character such as the curvature and tilt angle of the blades of fliers. Other structural properties such as precursor topology (inspired from different seeds) and overlaying blades (e.g., dandelion pappi) have a relatively small effect on the terminal velocity, and are therefore not discussed here.

Our modifications to the manuscript: On page 7, line 192, we added "Mesofliers with different 3D configurations exhibit a common dependence of v_T on η (Fig. 2d, S6), due to thick boundary layers at low Re."

Comment#3: *No mention is made in the paper comparing their design to the parachute of a dandelion pappus or a fluttering samara and I cannot find any data for their Ribbon fliers in the text. It seems from their analysis that samaras and pappi designs are less effective at reducing falling rate than the helicopter design, yet they are employed frequently in nature nonetheless.*

Our response: We thank the reviewer for this comment. The difference between the parachute design and helicopter design is in the rotating speed, and associated stability behavior as discussed in the manuscript. In additional work to address the referee's comment, we performed simulations to compare the parameters G_0 and G_1 for the parachute mode and rotational falling mode of design [3,H,0.75], as presented in Fig. R2c. The rotational falling mode has slightly smaller G_1 but higher G_0 than the parachute mode. This result suggests that the rotating speed increases v_T at low Re but reduces v_T at high Re. The fluttering behavior is considered an undesired chaotic mode, and is therefore not considered further here.

Our modifications to the manuscript: On page 8, line 214, we changed "Rotational behaviors (e.g., rotational speed ω_T) that follow from the 3D configuration (characterized by β) can confer kinematic stability. Analytical modeling (Supplementary Note 2), validated by CFD (Fig. S16), shows that $\omega_T \propto v_T/r$." to
"Rotational behaviors (e.g., rotational speed ω_T) that follow from the 3D configuration (characterized by β, rotation does not occur with $\beta = 0$) affect v_T by reducing G_1 and increasing G_0 (Extended Data Fig. 5), and by conferring kinematic stability. Analytical modeling (Fig. 2f, Supplementary Note 4) validated by CFD (Fig. S14) shows that $\omega_T \propto v_T/r$."

We added a subplot (c) in the previous Fig. S17:

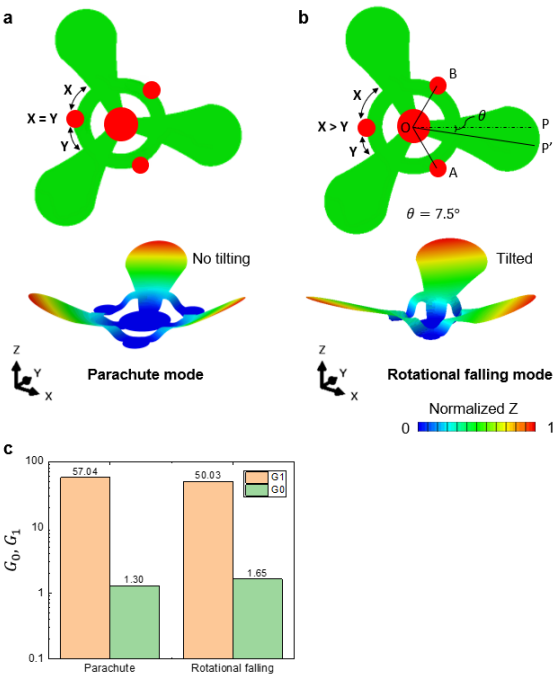

Extended Data Fig. 5. Mechanical simulation of a 3D microflier [3,H,0.75]. Schematic images of (a) a parachute design where the blades have no rotational tilting, and (b) a rotating flier design with rotationally tilted blades. (c) Comparison of G_0 and G_1 between the parachute mode and rotational falling mode.

Comment #4: *I would recommend that the authors connect their work to comparative work on wind dispersed seeds such as Augspurger AJB vol. 73, p353 (1986). In that paper different drag/lift mechanisms are compared for a wide range of taxa. Moreover Augspurger shows data for a number of seeds that fall at rates only slightly higher than the fliers shown in this paper, which would make a more sensible comparison than the non-wind-dispersed seeds (and snow) shown in Fig. 1(g). Additionally, the authors mention (without citation) in line 123 that wind dispersed seeds maximize stability and dispersal distance, yet their designs outperform these natural counterparts. I don't understand how this can be true if nature is truly maximizing the forces.*

Our response: We thank the reviewer for suggesting this reference and for providing additional insights on wind dispersed seeds. The focus of our work is on a narrow optimization around aerodynamics whereas evolutionary pressures in nature lead to seeds that adopt designs balancing many considerations in size, geometry, weight, metabolic expenditure, mechanical toughness, etc. As suggested, we included the reference and modified the Fig. 1(g) to include terminal velocities of helicopter type wind-dispersed seeds from the reference for a better comparison. We modified the manuscript as follows.

Our modification to the manuscript: On page 3, line 94, we changed "In this paper, we show that wind-dispersed seeds…" to
"In this paper, we show that wind-dispersed seeds[6]…"

On page 4, line 123, we changed "Wind-dispersed seeds adopt geometries that are shaped by forces of evolution to maximize dynamic stability and/or transport distance during passive free fall." to

"Wind-dispersed seeds adopt geometries that can be interpreted as evolutionary solutions to a physical problem governed by gravity and a sedentary lifeform, optimizing dynamic stability and/or transport distance during passive free fall[21]."

We replaced fig.1g with:

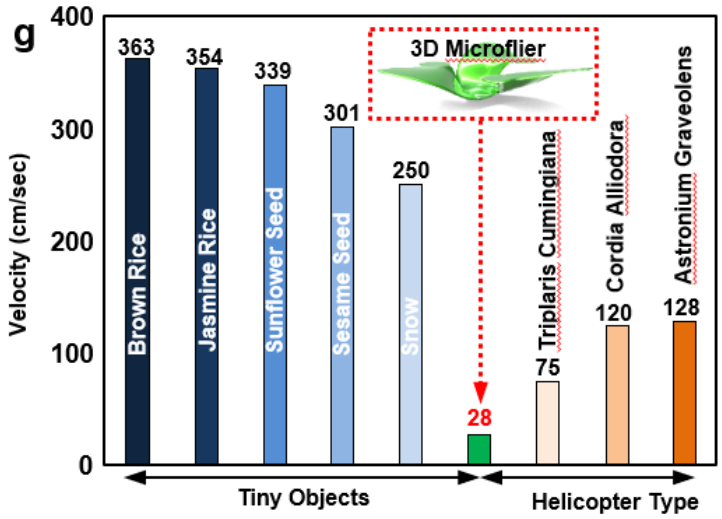

Figure 1. 3D microfliers inspired by wind-dispersed seeds. g, the terminal velocity of several small objects, helicopter typed wind dispersed seeds[6] and a 3D microflier [3, M, 0.4].

6. Augspurger, C. K. Morphology and dispersal potential of wind-dispersed diaspores of neotropical trees. *Am. J. Bot.* **73**, 353–363 (1986).
21. Greene, D. F. & Johnson, E. A. Seed Mass and Dispersal Capacity in Wind-Dispersed Diaspores. *Oikos* **67**, 69 (1993).

Comment #5: *In Figure 2, the captions for 2c and 2d are mismatched.*

Our response: We apologize for the mismatch. We corrected the captions for Figure 2c and 2d.

Comment #6: *On line 218, the variable Lambda_0 is not defined though it is defined in the SM. The paper would be more readable if it was also defined in the main text.*

Our response: We thank the referee for this valuable comment. We added the definition of Λ_0 in the caption of Figure 2.

Our modification to the manuscript: On page 20, line 537, we added "Stability can be analyzed by considering the flier as a rotating rigid body driven by forces associated with air flow and subjected to small perturbations ($\dot{\Lambda}_1 = \Lambda_0 \cdot 1s^{-1}$, where $\Lambda_{1,2}$ denote the perturbation angles in directions 1 and 2, Λ_0 denotes the amplitude) from an initial balanced state."

Comment #7: *In Figure S1 and Fig. 1a an array of flier designs is depicted. Is this truly a single photograph as the citations say? It seems like it would be difficult to achieve such clear focus over such a large depth of field. If these are composite photos the text should indicate that.*

Our response: We thank the reviewer for this comment. Yes, it is a single photograph, not a composite. We were able to obtain the large-depth field photography by using digital microscope (VHX-6000, Keyance) which has a naturally 20x larger depth of field than a conventional microscope.

Comment #8: *In Figure S8a the image is of a dandelion fruit or dandelion pappi, not simply seeds. The species for the feather depicted should also be listed if known.*

Our response: We thank the referee for this useful comment. We apologize for the mistake. We modified Fig. S8a and its caption as follows:

Our modifications to the manuscript: We modified Fig. S8 as Extended Data Fig. 4 and revised the caption:

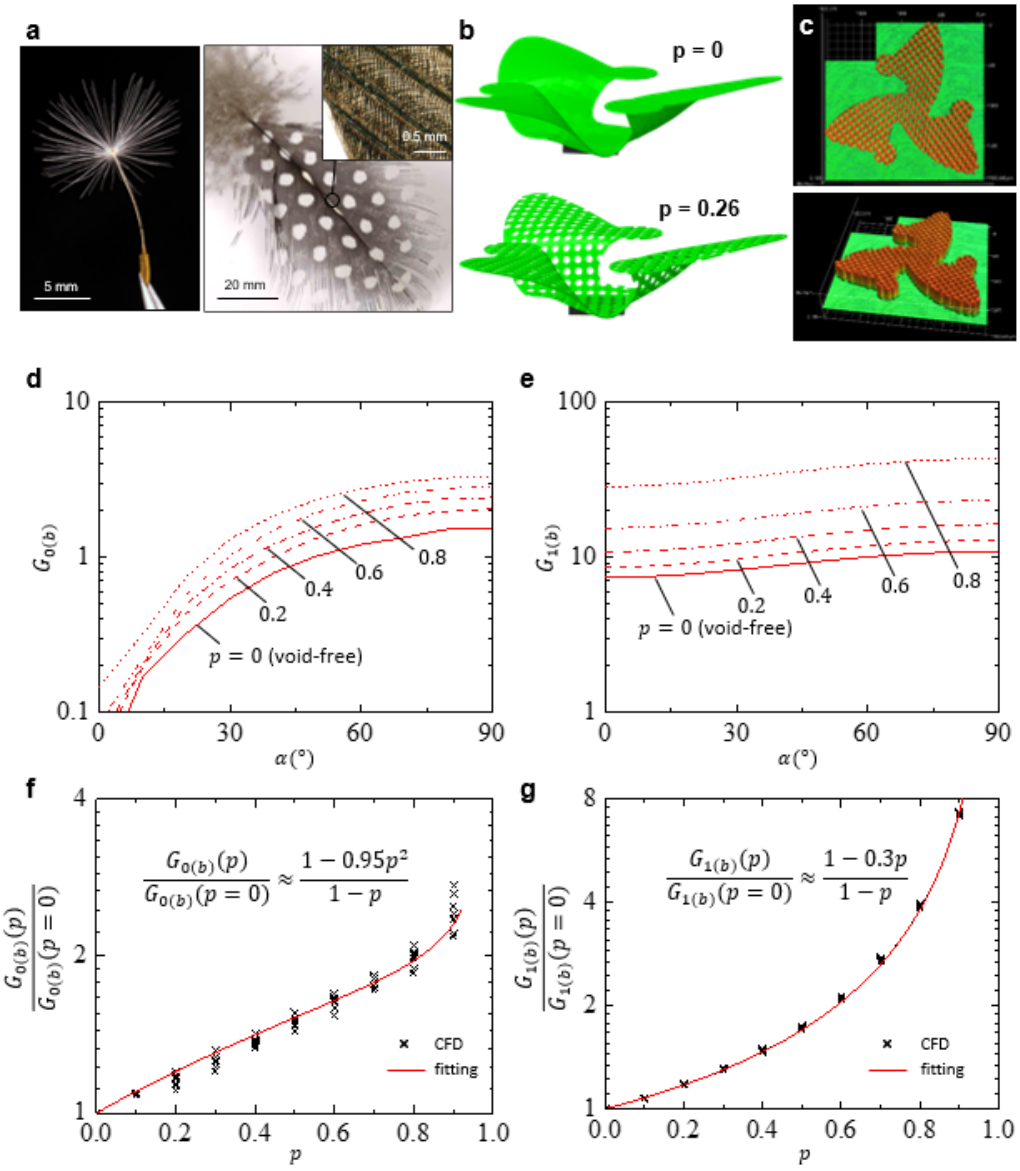

Extended Data Fig. 4. 3D microflier with porous design. (a) Inspiration of porosity from nature: optical images of a Dandelion pappi, and a guineafowl feather with locally enlarged view. (b) FE simulated configuration of a 3D void-free microflier ($p = 0$) and a 3D microflier of porosity design ($p = 0.26$). (c) Images of scanned thickness of a 2D precursor for a porous microflier, with top view

and perspective view, respectively. (d) $G_{0(b)}$ and (e) $G_{1(b)}$ versus the attack angle for various porosities. Normalized (f) $G_{0(b)}$and (g) $G_{1(b)}$ over their void-free values versus porosity, with the CFD values of various $\alpha \in [0°, 90°]$ and analytic fits.

Comment #9: *Equation S1.10 appears to have the lift and drag coefficients upside down in the middle fraction and should read C_L/C_D. Equation S1.13 also contains an error and, if we use the corrected L_D from above, the last term in parentheses should be (1+L_D^2)^{3/2}, not simply L_D. This equation is repeated in this incorrect form throughout the SM but does not seem to materially affect their analysis since empirical values for C_D are used rather than a value for L_D and Eq. S1.13*

Our response: We thank the referee for this useful comment. We apologize for the mistake. We corrected the equations in the SI notes.

Our modifications to the manuscript: In SI note 1, line 36, equation S1.10 modified to

$$\frac{\omega_T r}{v_T} = \frac{C_{L(b)}}{C_{D(b)}} = L_D, \qquad \textbf{(S1.10)}$$

L_D in SI note 1 after equation S1.13 corrected to L_D^2. Line 48, equation S1.13 changed to

$$F_z = \frac{1}{2}\rho v_T^2 \cdot [nbc] \cdot C_{D(b)} \cdot (1 + L_D^2)^{\frac{3}{2}}. \qquad \textbf{(S1.13)}$$

Line 51, equation of C_D changed to $C_D = C_{D,b} \cdot \left(1 + L_b^2\right)^{\frac{3}{2}}$. Line 60, equation S1.16 changed to

$$F_z = \frac{1}{2}\rho v_T^2 \cdot [nbc] \cdot \left(G_{0(b)} + \frac{G_{1(b)}}{\mathrm{Re}}\right) \cdot (1 + L_D^2)^{\frac{3}{2}}. \qquad \textbf{(S1.16)}$$

Line 64, equation S1.18 changed to

$$F_z = \frac{1}{2}\rho v_T^2 \cdot \pi r^2 \eta \cdot \left(G_{0(b)} + \frac{G_{1(b)}}{\mathrm{Re}}\right) \cdot (1 + L_D^2)^{\frac{3}{2}}. \qquad \textbf{(S1.18)}$$

Line 67, equation of G_0 changed to $G_0 = G_{0(b)}(1 + L_D^2)^{3/2}$. Line 69, equation of G_1 changed to $G_1 = G_{1(b)}(1 + L_D^2)^{3/2}$.

Reviewer Reports on the First Revision:

Referee #1 (Remarks to the Author):

Thank you for addressing all of my comments and making significant modifications to the main text and supplement. These changes have made the text clearer and the messaging more succinct, especially call outs to the extended figures and methods. References are fine and the data presented is clear. As stated in the first review, this work is novel and has impact for a wide scientific audience. The added experiments with chemical reagant sensors, the new supplemental table for potential onboard devices, and power transfer studies were well executed and helped demonstrate their usefulness for future distributed sensing and IoT applications. I have no further requests for more experiments or technical revisions.

Referee #2 (Remarks to the Author):

I appreciate the quick work the authors did in addressing my concerns with the first manuscript. This revision is a much more readable piece of work that in my opinion now highlights the most important results in the limited space the authors have. I also appreciate the effort the authors made to address each of my concerns in their response to my initial review. The work presented here is truly impressive and represents a tremendous amount of great work from a large and talented collaboration. I have no further suggestions for improvement.